Personal Navigation Using a Kinetic Model of Human Gait

A THESIS
SUBMITTED TO THE FACULTY OF THE GRADUATE SCHOOL
OF THE UNIVERSITY OF MINNESOTA
BY

Christopher J. Matthews

IN PARTIAL FULFILLMENT OF THE REQUIREMENTS
FOR THE DEGREE OF
MASTERS OF SCIENCE

Demoz Gebre-Egziabher, Adviser

December 2010

Abstract

Personal navigation concerns the tracking of human beings via devices carried or worn by individuals and presents a unique set of challenges in regards to navigation system and algorithm design. Many conventional position fixing and dead reckoning approaches tend to perform poorly given the requirements for personal navigation, which may consider GNSS-denied environments, a wide, highly dynamic range of motion, and low-cost and small form-factor sensor limitations. A novel approach to assisting or augmenting other navigation algorithms by employing a kinetic model of human gait is presented in this thesis. The kinetic model in concert with a single-axis accelerometer is shown here to comprise a virtual sensor capable of providing step size estimates in-situ for straight forward walking. Furthermore, the combination of the kinetic model and accelerometer yields a navigation solution of comparable or better performance when compared to a step counting dead reckoning approach. The derivation of this model is discussed, details of the experiments are given, and results are shown.

Contents

List of Tables

List of Figures

Chapter 1

Introduction

Personal navigation systems are devices intended to be carried or worn by an individual to provide a navigation solution. This differs from other common navigation systems in that the object they are intended to track is generally a human being as opposed to a vehicle such as an airplane or car. Unlike those vehicles, human beings exhibit diverse types of motion. Human motion is very dynamic, meaning we are capable of changing direction and velocity abruptly. In general, tracking human motion involves relatively low velocities but large accelerations occurring over short time scales.

1.1 Personal Navigation Applications

Personal navigation is a concept that is becoming a part of everyday life in part due to the popularity of smart phones and location based computing [1]. Thus, many phone manufacturers are producing products that contain GPS receivers, accelerometers, magnetometers, etc [2]. The availability of the technology to provide positioning information to the user has created a culture where consumers demand personal navigation information for a variety of tasks, i.e. finding directions to nearby restaurants.

Therefore, overcoming system limitations to provide users with personal navigation information in environments where many current systems are limited or unable to perform (i.e. indoors) poses a large potential reward with a large base of consumers already demanding more out of their smart phones.

Beyond the general consumer, personal navigation systems are of interest to first responders, law enforcement and military personnel. These types of users often require navigation information in new and unknown environments where infrastructure dependence becomes a major issue. Navigation duration may also be significantly longer than normal. Also, many applications where personal navigation systems are desired by these types of users involve safety-of-life [3, 4]. Thus, a demand for accurate, robust personal navigation systems exists.

Additionally, personal navigation technology can be employed in systems where the goal isn't necessarily to provide navigation information. These applications include, but are not limited to: assisting the blind or visually impaired, post-surgery monitoring of patients [5], motion capture for media applications, and gathering biometric information for individual identification [6, 7].

The design of a personal navigation system must take into consideration the environment in which the user is requiring a navigation solution. A navigation system designed for use outdoors may not work at all in an indoor or urban canyon type of environment. Personal navigation environments can contain magnetic anomalies that can distort measurements from magnetic compasses. They may contain physical or electromagnetic obstructions that hinder the use of radio frequency (RF) signals. The environment could even be moving in an inertial frame of reference, i.e. on board a ship or train.

Given the challenges associated with designing a personal navigation system that is robust to the various operational environments and provides useful, accurate and reliable navigation information to the user, a novel approach that takes advantage of available resources is proposed. In this thesis, a method of using human motion models as virtual sensors will be discussed. A motion model used to mathematically capture the motion (or lack of motion) of a person that is used with other available sensors to determine useful quantities that are useful is heretofore considered a virtual sensor. Specifically, this thesis will discuss the fusion of a kinetic model of the human gait with a single, ankle mounted accelerometer to form a virtual step size sensor capable of providing accurate, reliable step sizes estimates to a navigation system.

1.2 Personal Navigation Methods

Navigation solutions generally use one of two fundamental ways of determining position and velocity. *Position Fixing* methods are most often chiefly concerned with positioning, or directly determining the position of a body in space. Many operate at a high enough rate to provide velocity from the time rate of change of position or have an alternative means of velocity determination i.e. examining the doppler shift of a radio signal carrier. In contrast, *Dead Reckoning* methods determine position by measuring the change in position or integrating velocity or acceleration measurements. Thus, the new position is determined by adding the change in position to the previous position.

Many sensors suitable for use in personal navigation have been developed. However, these sensors need to generally be small, light-weight, low-cost and low-power in order

to be employed in different personal navigation applications. These requirements generally mean poor performance is expected out of the sensor. Therefore, it is desired to design a navigation system that can somehow take advantage of a certain method's strengths while minimizing the effect of its shortcomings, and taking into consideration the many different and dynamic ways in which a person moves and assessing the robustness of the design in different environments. Thus, state-of-the-art navigation systems often produce *Blended Solutions* in which both methods can be employed using multiple sensors and position and velocity are estimated by blending different solutions in an estimator such as a Kalman filter [8].

1.2.1 Position Fixing Solutions

Position fixing navigation systems are those that involve sensors that directly provide measurements from which a user's location can be estimated. Many current personal navigation systems rely on information from satellite signals from Global Navigation Satellite Systems (GNSS) like GPS operated by the United States or GLONASS operated by the Russian Federation [8]. These systems acquire information via RF signals from a number satellites in view and use a form of multi-lateration to determine the user's position. In addition, GNSS is often used as a means of determining time [9]. Many receivers use the doppler shift of the RF carrier to determine the user's velocity as well [10]. Other RF signals can be used in much the same way to provide a personal navigator with a way of measuring position, velocity and time. Two such examples are Wi-Fi and Ultra-wide Band (UWB) signals [3].

The main advantage of the position fixing method is that the errors in the navigation solution do not grow with time, which is important in situations where the duration of use is long. There is also generally no need to initialize the system, meaning a user can simply turn the device on and they will begin receiving positioning information.

The major drawback of these systems is that they are infrastructure dependent. If radio signals are to be used they must be available and not impaired, obstructed or interfered with in order for the navigation system to be able to use them. This means that settings like urban canyons or inside buildings presents a challenge to acquire signals from e.g. GPS. Although GNSS signals are spaced based and therefore widely available in open areas, other potential signals like Wi-Fi or UWB must be available on-site. The implies a pre-prepared infrastructure which is not always practical (e.g. military operations in remote areas).

1.2.2 Dead Reckoning Solutions

Dead reckoning, or deduced reckoning, solutions are obtained from a history of change in position, velocity, or acceleration measurements iteratively added to a known initial navigation solution or initial condition. Inertial navigation, or the use of accelerometers and gyroscopes to capture acceleration and rotation rate information, is perhaps the most popular and widespread method for dead reckoning applications. Other sensors for doing dead reckoning include pedometers, odometers, Doppler radars, laser radars (LIDAR), barometric altimeters, magnetic compasses, celestial cameras, etc [8].

The drawback of dead reckoning is that the errors associated with computing a navigation solution grow with time. For example, the use of an Inertial Measurement Unit (IMU) as a dead reckoning navigation sensor package requires that the angular rate sensors (gyroscopes) be integrated to produce an attitude solution which is then used to align the acceleration sensors (accelerometers). The acceleration measurements are then integrated twice to arrive at position. Therefore, any error in the angular rate measurements contribute a t^3, or cubic-in-time, error growth rate. This means that

any errors in a dead reckoning measurement must be small, otherwise the position solution will degrade in accuracy very quickly. In the case of using a relatively cheap commercial grade IMU, the position error may exceed 100 meters after a minute of navigating [11]. These errors are usually stochastic in nature, and, thus the time dependent growth of these errors is a *random process*.

Although the time dependent errors are a significant issue with dead reckoning sensors, there are a few advantages to using them as well. First, dead reckoning sensors normally do not require any signals or external cues from other systems, therefore they are self-contained. Second, there are many low-cost, small sensors suitable for dead reckoning that are commercially available in Micro Electromechanical Systems (MEMS) form factors. Finally, the data rate is generally very high, often faster than 50 Hz, which is advantageous for sensing the motion of highly dynamic systems like human beings.

1.2.3 Blended Solutions

A blended navigation solution is one which fuses dead reckoning and position fixing solutions from different sensors. The navigation output of the system is the result of an estimator such as a Kalman Filter which blends the two navigation solutions. For example, in an inertial navigation system there may be position, velocity, attitude, accelerometer bias and gyro bias error states where their values at a given instant in time are used to attempt to correctly calculate a navigation solution. The estimator can use other sensors, e.g. position information from a GPS receiver, to calculate these states. If the estimator is designed appropriately for the problem, the resulting navigation solution is an improvement on the initial solution produced from e.g. an inertial navigation system.

1.3 Personal Navigation Applications

Personal navigation is a concept that is becoming a part of everyday life in part due to the popularity of smart phones and location based computing [1]. Thus, many phone manufacturers are producing products that contain GPS receivers, accelerometers, magnetometers, etc [2]. The availability of the technology to provide positioning information to the user has created a culture where consumers demand personal navigation information for a variety of tasks, i.e. finding directions to nearby restaurants. Therefore, overcoming system limitations to provide users with personal navigation information in environments where many current systems are limited or unable to perform (i.e. indoors) poses a large potential reward with a large base of consumers already demanding more out of their smart phones.

Beyond the general consumer, personal navigation systems are of interest to first responders, law enforcement and military personnel. These types of users often require navigation information in new and unknown environments where infrastructure dependence becomes a major issue. Navigation duration may also be significantly longer than normal. Also, many applications where personal navigation systems are desired by these types of users involve safety-of-life [3, 4]. Thus, a demand for accurate, robust personal navigation systems exists.

Additionally, personal navigation technology can be employed in systems where the goal isn't necessarily to provide navigation information. These applications include, but are not limited to: assisting the blind or visually impaired, post-surgery monitoring of patients [5], motion capture for media applications, and gathering biometric

information for individual identification [6, 7].

1.4 Problem Statement

The purpose of this research reported in this thesis is to make an initial attempt at using human motion models as sensors in personal navigation systems. A related objective is to determine the type and number of additional sensors that must be "worn" by a person if they are to leverage the information of a human motion model in providing a navigation solution.

This approach to obtaining navigation information is novel in that it takes advantage of a couple of details. First, a human motion model when used as a virtual sensor is ubiquitous and therefore behaves the same regardless of the user's external environment. Second, the details of human motion are dictated by measurable physical characteristics (e.g. height, limb lengths) that limit the motion possibilities. Therefore, motion models when used as virtual sensors will provide outputs that are constrained.

1.5 Thesis Organization

To this end, the organization of this thesis is as follows:

- Chapter 2 discusses the analysis done to break down and understand a particular aspect of human motion that is of interest: the gait.
- Chapter 3 contains the details of the derivation of the kinetic model of human gait used.

- Chapter 4 explains what is involved in the process of solving and integrating the equations of motion to arrive at an estimate of step size.
- Chapter 5 discusses the different validation and performance assessment experiments done.
- Chapter 6 talks about the different sources of error involved and presents a sensitivity analysis.

Chapter 2

Analysis of the Human Gait

Humans, as bipedal creatures, move via a gait. A gait is defined as a manner of moving on foot and running, walking, skipping, etc. are all different modes of the human gait. These different types of motion often display a pattern behavior. For example, when a person is walking at a leisurely pace it is observed that all of their steps are of approximately the same size, and the cadence, or rate of repetition, is also approximately constant. This results in a person walking at a relatively constant speed [12]. The natural walking pattern of a human may vary slightly depending on the situation. For example, people walk differently while in a hurry than while on a leisurely stroll. Additionally, a person's size, mass distribution, level of fitness, etc. have a significant effect on their gait profile. For example, an athlete walks differently from a non-athlete; taller persons have a longer natural stride length; larger feet require more articulation at the knee so the foot can clear the ground when a leg swings forward.

Despite the person to person differences, consistent motion patterns exist for most if not all modes of bipedal motion. An individual's personal walking pattern is a variation on this overall basic pattern. The existence of a personal walking pattern that is similar across individuals means that a generic model only needs to be devel-

oped that includes a set of parameters, such as limb lengths, which can be adjusted to accommodate different individuals. Identifying these patterns alone can provide meaningful information to the personal navigator [13, 14]. The model presented in this thesis attempts to do that.

2.1 The Passive Walker

The design of the human body allows for efficient means of motion that are either built into instinct from birth or learned at an early age [15]. An example is the heel-to-toe rolling motion the feet and ankles make as we walk. From this, it is reasonable to infer that when a person is moving (i.e. walking) and has established forward momentum, the body does the least amount of work possible to continue the motion. Understanding this point allows us to intuitively relate the complex biomechanical human walking process to a simple passive walker [16].

Passive walkers are machines often built for hobby or teaching robotics that consist of two pendulums (legs) connected at a pin joint that substitutes for a hip. Two examples of such machines are given in [17, 18]. If given a slightly downhill surface, a gentle swing and push to start, the walker is capable of continuing a walking motion for many steps. Gravity is the only force necessary to maintain the motion. Gravity provides compensation for energy loss due to impact at each step and friction in the joints. Taking the inclined surface away creates a need for input forces and torques to maintain the energy balance. The muscles in the human body provide these input torques. While these applied torques are complex in nature, analyzing the passive walker's dynamics suggests that the active torque contribution to the system is small compared to gravity. Therefore, it can be said that straight-forward human walking

is passive to some extent [19]. This conclusion forms the basis for the design of the kinetic model discussed in this thesis.

2.2 Anatomy

Though a classic passive walker is a gross simplification of the human anatomy, its success at producing human gait-like motion suggests that certain anatomy related assumptions and simplifications can be made in order to assist the modeling process. Other than brief instances where both of a walking person's feet are in contact with the ground, one leg is supporting the weight of the body while the other is swinging forward. The leg that swings forward and avoids contact with the ground is defined as the *free leg*. The leg supporting the weight of the body and counter-rotating above the foot's contact with the ground like an inverted pendulum is called the *stance leg*. Figure 2.1 depicts this difference. Over the course of a stride, the free leg ceases to be in contact with the ground until the stride is completed. At this point, the free leg transitions to become the stance leg. Once that same leg is done supporting the stride of the other leg, the role switches again. In this way, the gait is achieved.

In this thesis, the upper leg of the human body between the knee and hip joints is referred to as the *thigh*. The human thigh contains one bone, the femur, and several large groups of muscles that produce a majority in the movement of the hip and knee joints. Much of the work done by the human body to create or maintain the gait is done by these muscles. In contrast, the lower leg is referred to as the *shank* and contains bones called the tibia and fibula. The patella, or commonly the knee cap, is over the knee joint just above shank. The front, or anterior, of the shank is commonly referred to as the shin, while the rear or posterior, is called the calf. The muscles

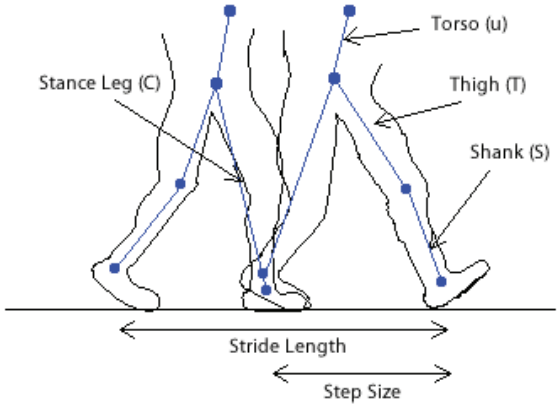

Figure 2.1: The above depicts the different limbs as they have been defined for development of the kinetic model discussed in this paper. Additionally stride length and step size are visually defined.

associated with the shank are responsible for moving the foot.

The feet of a human being are complex systems in their own right. Each human foot and ankle system has twenty-six bones and thirty-three joints, of which roughly twenty significantly articulate. During the gait muscles in the foot articulate the anatomy in such a way as to provide a stable base for the rest of the human body. Thus, many complex interactions occur just to provide a person with balance during walking. Modeling such a system in a detailed sense is a unique challenge, however, it is an unnecessary one. From a big picture view of the role of the foot, it is primarily providing a stable base so that the upper leg and rest of the body essentially rotates about while the motion of the body of as a whole progresses. This is akin to thinking of the human body as a rimless wheel during walking, where the tips of the spokes are the feet; the body rolling along over the spokes' short term contact with the ground [19]. Viewing the role of the foot in this way allows for the assumption that it can be ignored in the model and the end of the lower leg can be considered the "foot."

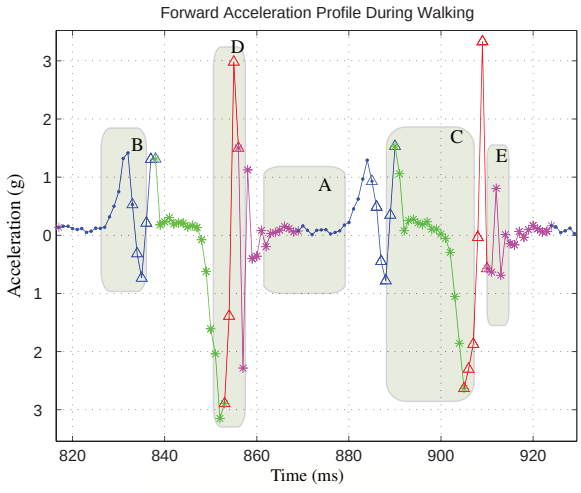

Figure 2.2: The gait pattern is shown from a history of a_x measurements with five distinctive events highlighted. They are A: Stance/Support, B: Toe-Off, C: Swing/Crossover, D: Heel-Strike, and E: Double Support.

2.3 Gait Events

In examining gait patterns, it is natural to begin to break the cycle down into different key events that explain how different details arise that ultimately contribute to the movement of the system as a whole. Figure 2.2 was constructed using data collected by a system discussed later in this chapter. The figure contains certain highlighted parts of the acceleration profile seen with the x-direction accelerometer at the ankle. These segments of the acceleration profile are different gait events.

With something as detailed and complex as human walking, researchers in the subject area tend to break the pattern down differently based on the focus of the research. For the purposes of this thesis, five different gait events will be identified. These

events are: single support, toe-off, swing, heel-strike and double support. It is important to note that the sections of the acceleration profile highlighted in Figure 2.2 may suggest certain instantaneous events, e.g. heel-strike, that are considered here to be brief processes instead intending to refer to the position, velocity and acceleration of the ankle around a given instant in time.

Being able to successfully identify when a certain gait event is occurring involves a significant qualitative analysis be quantitatively related to measurements from e.g. an IMU. To enable this process the gait events as they relate to the acceleration profile in Figure 2.2 will next be analyzed in more detail. For the purposes of this discussion, the focus will be placed on one leg of a bipedal walker to hone in on the different roles a particular leg plays during the evolution of a stride.

2.3.1 Single Support

A leg is said to be in single support while it is the only leg in contact with the ground. Thus, the leg in single support is the stance leg. The left-hand plot of Figure 2.3 highlights the portion of the x-acceleration profile at the ankle that corresponds to single support. The ankle of the stance leg is seen to accelerate and decelerate in relatively low magnitude. This is because the foot of the stance leg is attempting to provide a stable base for the rest of the stance leg to rotate over.

The right-hand plot in Figure 2.3 shows that the ankle of the leg of interest does not move much in single support, however the rest of the leg does. This is seen by the black overlayed plots of the hip and knee joints of the leg of interest that are also given in green and red respectively. The legs of the walker are also visualized at the beginning and end of single support on the plot with the leg of interest appearing in

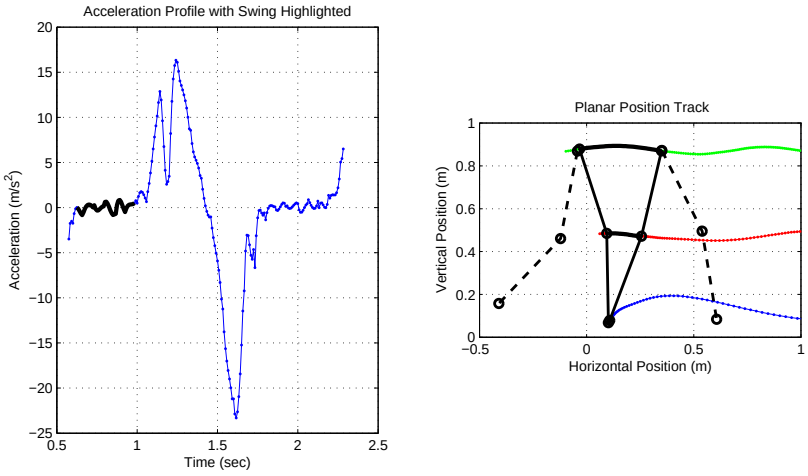

Figure 2.3: The single support gait event is highlighted with a black overlay on the acceleration profile (left) and visualized with a walking figure on the planar joint trajectory plot (right).

solid black. It can be seen that the stance leg approximately rotates about the ankle while the free leg appears to be swinging forward.

2.3.2 Toe-Off

Toe-off refers to the process of the foot of the leg of interest articulating in the process of leaving the ground. Several interactions occur to make this event happen. The free leg interacts with the ground at the start of toe-off, and thus a significant portion the momentum of the walking system is transferred to the stance leg, which now trails the free leg. Thus, the leg of interest switches roles and transitions from being the stance leg to being the free leg. As this happens the continued momentum driven forward motion of the hip and upper body effectively pulls the foot of the leg of interest off the ground. The muscles in the shank assist in this process, in turn rolling the knee forward and slightly downward as the foot rotates so that progressively the ball of the

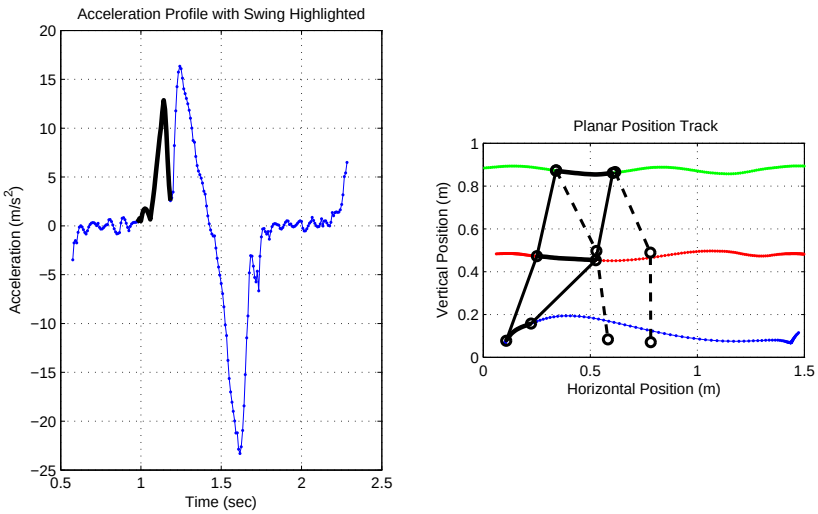

Figure 2.4: The toe-off gait event is highlighted in black overlay on the acceleration profile (left) and visualized start-to-finish with a walking figured on the planar joint trajectory plot (right).

foot remains in contact, then finally only the first few toes are in contact. Ultimately the foot on the leg of interest leaves the ground.

The planar position track on the right of Figure 2.4 visualizes this process. The knee is shown to move significantly more than the ankle in the horizontal direction. This is because the knee must move and articulate significantly to allow the base of the foot to rotate up onto its ball. As the knee continues to drive forward the foot is picked up off the ground.

The corresponding accelerations during toe-off show a sharp peak with a significant positive acceleration. The positive trending acceleration of the profile at this point is a manifestation of the momentum carryover of the system, while the negative trending acceleration after the peak captures the pick-up of the foot as it rotates up, onto and eventually off of the toes.

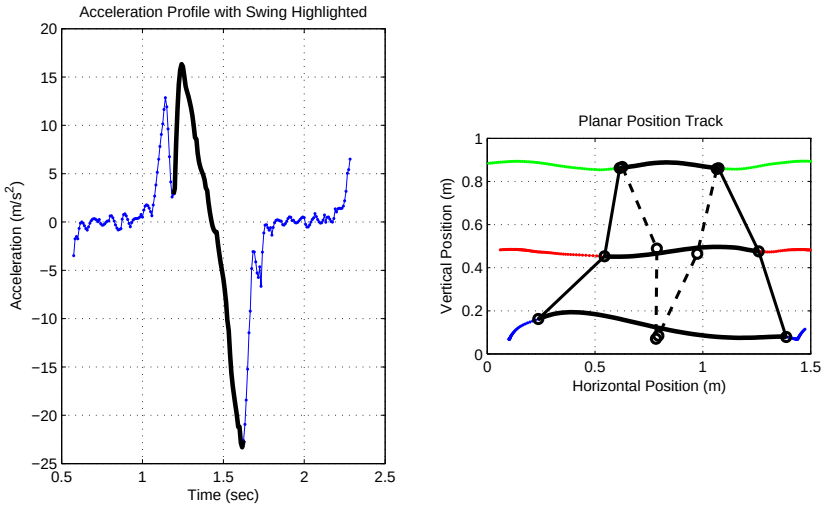

Figure 2.5: The swing gait event is highlighted in black overlay on the acceleration profile (left) and visualized at the beginning and end with a walking figured on the 2D joint trajectory plot (right).

2.3.3 Swing

The swing is the portion of the gait cycle where the ankle of the leg of interest will translate through space the most significant amount. This is seen in Figure 2.5 where the right hand plot shows the ankle moving almost 1.2 meters horizontally. Thus, the vast majority of the motion of interest is during the swing, as the counter rotation of the free leg relative to the stance leg creates the stride. Also of note is that the hip translates the least amount during this gait event.

The acceleration plot on the left-hand side of Figure 2.5 shows a significant positive acceleration at the beginning of the swing, causing the forward motion. As the swing progresses, the acceleration becomes a deceleration, arresting the motion of the leg in

anticipation of the end of the stride. Therefore, as the free leg swings forward, there comes an instant in time where the leg slows its rotation with respect to the stance leg and the ankle's velocity decreases rapidly. At the end of this process, the foot of the leg of interest will encounter the ground once more.

2.3.4 Heel-Strike

The heel-strike is perhaps the easiest gait event to detect with a set of accelerometers. This is because the sudden stoppage of motion at impact causes an energy transfer to occur that will physically move the sensor's mounting system. Thus, the heel-strike events look different between the accelerometer captured profile in Figure 2.2 and the motion capture acceleration profile in Figure 2.6. The heel-strike detected in Figure 2.2 by the accelerometer has a large spike that is also present in the other two accelerometer axes. This makes step detection and counting straight forward as a user simply needs to wait until a spike appears in the data to signal a step has occurred.

However, what has really occurred is the foot/ankle region has strongly decelerated and then has quickly stopped accelerating all together. This is seen Figure 2.6. With the acceleration driven to zero after the impact with the ground, the momentum still moves the walker slightly, though energy has been lost. This loss of energy destabilizes the walking system and would normally cause a biped to cease walking and essentially fall over. To overcome the energy loss at heel-strike, the human body's nervous system orchestrates the contraction of different muscles in a way that will add energy to make up for the loss throughout the gait process.

Although it may be the case that the heel is not the part of the foot that strikes first,

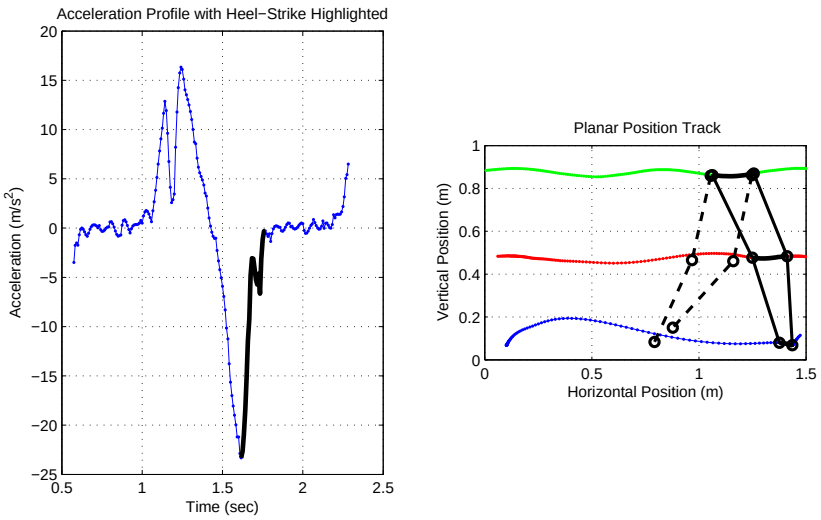

Figure 2.6: The heel-strke gait event is highlighted in black overlay on the acceleration profile (left) and visualized with a walking figured on the 2D joint trajectory plot (right).

this gait event is still defined as such since it is the most common way the free leg foot will interact with the ground post-swing. It is also the most efficient means of interacting with the ground, as the design of the foot allows for a rolling-like interaction with the ground as the foot settles after impact. This means less energy is lost in the process compared to a flat footed impact with the ground.

2.3.5 Double Support

Double support refers to the brief period of time in the gait cycle when both feet are in contact with the ground. During this event, there is little to no acceleration of the ankle/foot. For walking persons, the duration of double support is roughly inversely proportional to the speed. In order for a biped to move faster, the stride lengths have to increase and the cadence or repetition of the gait must also increase. As

this happens, double support decreases in duration as the new strides with opposing legs require more of a cycle's time. Therefore, at slow walking speeds when double support is more prevalent, the body is allowed to use the brief time to stabilize and adjust to the demands of the next step that is about to happen. Double support is not present in running.

2.4 Gait Variability

Stride-to-stride variations exist even when external conditions do not change due to small fluctuations in the human anatomy. A person walking straight forward at an approximately constant speed on a flat surface clear of obstacles will not make identical strides. Small variations in the biomechanical process of the gait, i.e. different portions of muscles firing out of sequence, will cause step sizes, among other things, to change slightly if not significantly from step to step [20].

Much of the natural gait variability that leads to small but significant step size changes during normal gait is derived out of the soft tissue nature of the body. When also considering sensor errors, it is no wonder that capturing two nearly identical steps is practically impossible. With that in mind, it is important to design a system of capturing the dynamics of the human gait in-situ in order to capture the small changes from e.g. step to step.

Figure 2.7: Photo of the Microbotics, Inc. MIDG II INS/GPS sensor [21] secured to an elastic band and worn above the ankle. Data from the MEMS accelerometers inside the MIDG are used with the kinetic model to estimate step size in-situ.

2.5 Data Collection Hardware

A Microbotics, Inc. MIDG II MEMS Inertial Navigation System/GPS sensor package [21] was attached to an elastic band and worn just above the ankle as shown in Figure 2.7. The MIDG contains a triad of accelerometers, a triad of rate gyros, a triad of magnetometers, and a GPS receiver. The accelerometers, gyros, and magnetometers were aligned such that their parallel axes were oriented as depicted in Figure 2.8. The accelerometers provided *specific force* measurements, which is to say they measured the acceleration components of the limb to which they were attached plus the local gravitational acceleration.

Removing the gravitational acceleration component in the accelerometers is a challenge because of the relatively poor rate gyro performance making attitude measurements severely erroneous after a short time. Thus, the forward, x-direction accelerometer was primarily used for gait analysis since the gravitational contributions to the accelerometer signal were minimal during walking and the forward acceleration captured was in the direction of travel.

Motion data was also collected using a 12-camera Vicon MX system that employs a Plug-in-Gait marker set and model to generate kinetic and kinematic data [22]. An experimental volunteer would have several reflective markers placed in different specified locations on their body. The cameras track the locations of these markers and provide the test administrators with x-y-z position information that is accurate to the millimeter or better. The marker locations were such that the locations of the joint centers of the left and right hip, knee and ankle joints could be calculated and provided as another measurement output of the system.

The Vicon motion capture data used for analysis was supplied from a large database of volunteer subjects with "normal gait" having worn the reflective markers and having been instructed to walk several steps at different speeds. Each data set was processed using a plug-in gait model in such a way as to provide the 3-D position histories of the joint centers for both the left and right hip, knee and ankle joints of a particular individual. From those joint trajectories, other useful information was reconstructed. This additional synthesized data included joint velocity and accelerations, limb lengths, limb angles with respect to the vertical, and synthetic accelerometer measurements which mimic the specific force outputs of an IMU attached just above a subject's ankle. Note: due to the process of reconstructing acceleration and velocity information, some errors are introduced. These are typically small but tend to be more prevalent in instances where a particular joint is moving very little or not at all, e.g. the ankle during single support.

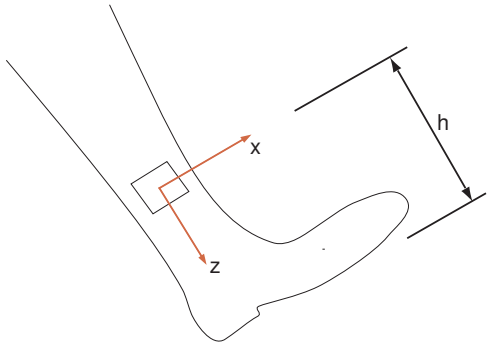

Figure 2.8: Diagram of MIDG sensor axes orientation as it is worn at the ankle. The positive y-axis is defined out-of-the-page.

2.6 Gait Pattern Experiments

Data was analyzed from sensors worn just above the ankle as opposed to a shoe mounted location. In addition to the high-ankle being an easy and convenient location to mount a sensor, it also takes out the error associated with the articulation of the ankle joint and the noisy motion of the foot that can be difficult to characterize. This reduces the systematic errors associated with how the sensor is attached to the test subject, while enhancing the signal to noise ratio and producing more consistent walking patterns in the data. This does, however, mean that the distance h in Figure 2.8 (a scale factor associated with the sensor's distance to the bottom of the foot) needs to be taken into account in the analysis.

Initially in order to understand the gait profile, experiments were conducted that consisted of 10-20 steps at different step sizes of a specified length and additionally walking was done at different specified tempos or cadences. This was achieved using guides marked by tape or chalk on the ground for step size. For cadence, tempo references between 80 and 132 beats per minute were given before walking. Data was collected at different walking speeds as a result of the varied step sizes and cadences.

While measurements were done under various conditions, the basic acceleration profile remains largely unchanged. A typical acceleration profile for the forward, x-direction is shown in Figure 2.2.

Chapter 3

Kinetic Model of Human Gait

A kinetic model of human gait is derived in this chapter and used as the equations of motion that are employed to capture the walking motion mode. The use or modification of this model to capture other motion modes such as running is a subject of possible future work.

At the foundation of this model is the following key assumption: The gait cycle is that of a passive walker. This implies that gravity and inertia are the major contributors to motion. However, there are some forces and moments that we cannot accurately model or directly measure. Of these "other forces and moments," the musculoskeletal activity of the human body that generates, controls and maintains motion dominates. However because of how similar the motion of a completely passive walker is to every day human walking, these other forces and moments typically contribute little to the gait cycle. This was verified by data from our validation experiments and does form the basis of the theory for developing our equations of motion in the kinetic model.

3.1 Modeling Assumptions

Straight forward human walking is approximately planar. Therefore, the model is derived using a 2-D assumption with forward and vertical directions, ignoring any sideways, translational motion. This means that we will assume that the limbs of the walking model defined will translate and rotate through space attached to the 2-D plane depicted in Figure 2.1.

Additionally, we observe in experiments discussed later that the knee of the stance leg does not articulate significantly during walking. During a relatively long stride the stance leg knee has been seen to only bend a maximum of 10-15 degrees. Thus we will assume that the stance leg is straight in the development of our model. This simplification means that we can model the gait using only three limbs, considering the stance leg as one limb along with the thigh and shank of the free leg.

Approximately 60 percent of the mass of the human body is above the waist. The presence of this mass does significantly contribute to the dynamics of the gait. However, during walking the neck and torso do not articulate in a wide range of motion. The amount of trunk rolling and yawing is small and there is very little pitching, i.e. bending the spine forward or backward. In the model derived here, the swinging of the arms is completely ignored and the upper body is modeled as a frustum of significant mass that maintains a constant angle with the vertical.

A human leg is a complex biomechanical system consisting of heavy soft tissue and a rigid skeleton. Each leg has three major joints: the hip, knee and ankle. All three joints are very complex in reality. Accurately modeling their dynamics is a daunting task itself. However the aim of this research is to identify external physical quantities

to assist a navigation system and as such modeling these complex systems as simple hinge joints is admissible.

In addition, modeling the upper and lower legs as rigid frustums is done to take into account the stability the bones provide while using the variably distributed mass of the frustum to capture the significant mass of the muscles and other soft tissue.

While the angle of the terrain on which the person is walking, γ, is also important to consider, in the model that follows it is assumed that γ is zero. Thus the terrain is flat.

3.2 Modeling Approach

The Newton-Euler approach was used to deriving the equations of motion [25]. These equations are the moment equations for the free body diagram shown in Figure 3.1. The diagrams consist of the limbs of interest that we have defined: The stance leg, upper body (torso), free leg knee and free leg shank. The foot of the stance leg is also modeled and provides for the location where the ground reaction force, R, is applied to the stance leg.

The passive dynamics include the contributions from gravity and inertia. In the free body diagram in Figure 3.1 the forces associated with gravity acting at limb centers of mass G_L, G_u, G_T and G_S. These centers of mass are also where the effective accelerations a_L, a_u, a_T and a_S act. The system inertia is captured in the angular momentum derivatives, $\dot{H}_L$, $\dot{H}_T$ and $\dot{H}_S$.

However, real human walking is not passive, and therefore we include internal mo-

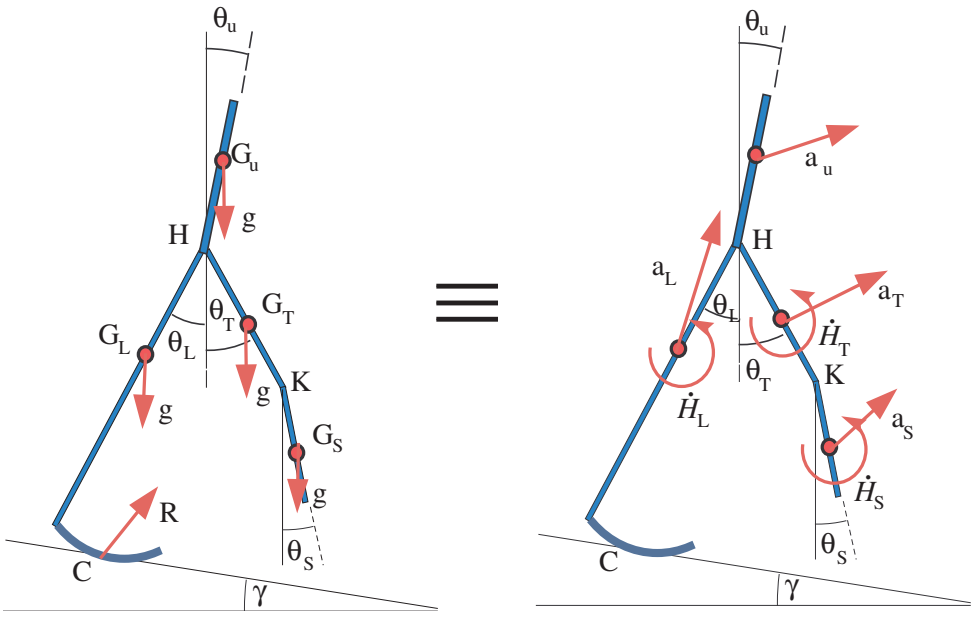

Figure 3.1: The free body (left) and effective force (right) diagrams drawn for the kinetic model. The problem is analyzed in 2-D with straight forward walking assumed.

ments at the hip and knee to effectively model the contributions the musculoskeletal system on the motion of our walker. As the moments applied at the hip and knee are internal, they appear in Figure 3.2 and Figure 3.3 respectively but not in Figure 3.1.

3.3 Model Parameters

In addition to what is shown in Figure 3.1 the following parameters are part of the kinetic model:

- ℓ: stance leg length.
- d: thigh leg length.
- ρ: distance to the stance leg center of mass, G_L, from the ankle joint center.

- τ: distance to thigh center of mass, G_T, from the hip joint center.
- σ: distance to shank center of mass, G_S, from the knee joint center.
- η: distance to upper body center of mass, G_u, from the hip joint center.
- r_L: distance from stance leg ankle to ground contact point.
- k_L: stance leg radius of gyration.
- k_T: thigh radius of gyration.
- k_S: shank radius of gyration.
- μ_L: mass of the stance leg.
- μ_u: mass of the upper body.
- μ_T: mass of the thigh.
- μ_S: mass of the shank.
- θ_u: angle of the torso with the vertical (radians).

The shank length is not defined because it is assumed to be the difference of the thigh length from the stance leg length, $(\ell - d)$. Normalization of these parameters is defined by dividing the true quantity by some physically measured reference. The length reference is defined as a person's measured leg length and the mass reference is given by a person's total body mass–two easily obtained quantities. In this way, all of the distances defined are unit-less because they have been normalized by the measured leg length. Additionally, the masses of the different limbs are unit-less because they have been normalized by the total body mass. This normalization is important to avoid the use of the wrong units.

With the exception of θ_u, which is determined by an educated guess, and the limb lengths, which can be physically measured, most of the parameters in the model are determined based on empirical anatomical trends that have been discussed in gait research and other places in the medical community. These trends are discussed in [23, 24]. The gravity vector, $\mathbf{g}$ is also scaled and has a magnitude of $(g/\hat{\ell})$ where the acceleration due to gravity in meters per second squared has been divided by the measured leg length, $\hat{\ell}$, in meters.

3.4 Equations of Motion

The generalized coordinates of the system are the angles that each articulating limb makes with the vertical. Again it is assumed that the angle of the torso with the vertical does not change and is known. The generalized coordinates are unknown as are the associated angular velocities. Thus, the state vector is defined as:

$$\mathbf{x} = \begin{bmatrix} \theta_L & \dot{\theta}_L & \theta_T & \dot{\theta}_T & \theta_S & \dot{\theta}_S \end{bmatrix}^T \tag{3.1}$$

The equations of motion are derived by considering summation of moments about different points. For example, in referring to the free body diagram in Figure 3.1, a moment equation can be written about point C. This equation,

$$\Sigma \mathrm{M}_C = \mathbf{r}_{CG_u} \times \mu_u \mathbf{g} + \mathbf{r}_{CG_L} \times \mu_L \mathbf{g} + \mathbf{r}_{CG_T} \times \mu_T \mathbf{g} + \mathbf{r}_{CG_S} \times \mu_S \mathbf{g} \tag{3.2}$$

$$= \mathbf{r}_{CG_u} \times m_u \mathbf{a}_u + \mathbf{r}_{CG_L} \times \mu_L \mathbf{a}_L + \mathbf{r}_{CG_T} \times \mu_T \mathbf{a}_T$$

$$+ \mathbf{r}_{CG_S} \times \mu_S \mathbf{a}_S + \dot{H}_L + \dot{H}_T + \dot{H}_S$$

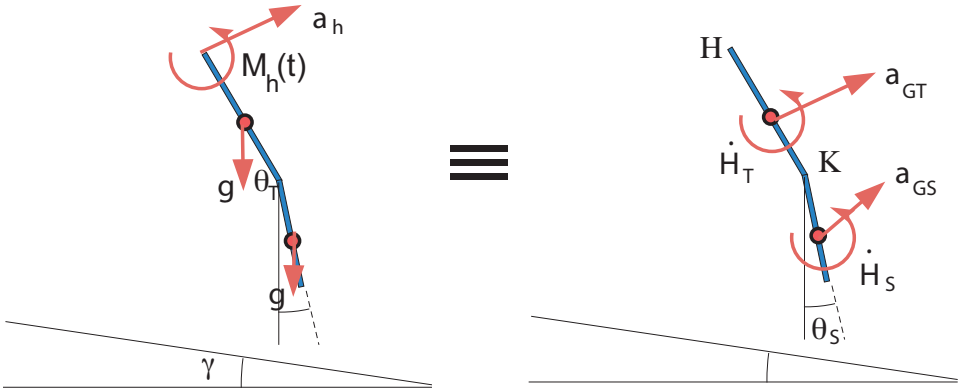

Figure 3.2: The free body and effective force diagrams are shown for kinetic model that has been truncated to only show the thigh and shank. This allows for the writing of Figure 3.2.

contains the gravitational contributions on the left hand side corresponding to the moments on the free body diagram, while the right hand side features the angular momentum derivatives and the effective forces present on the effective force diagram. The vectors $\mathbf{r}$ are the distances as indicated by the subscripts, where e.g. $\mathbf{r}_{CG_T}$ is the vector from point C to the center of mass of the thigh, G_T.

To get additional equations of motion, other points on the free body diagram are considered. Specifically, points H in Figure 3.2 and K in Figure 3.3 are considered. The moment equation about H incorporates a model for a locally applied moment. This moment is assumed to have the following form:

$$M_h(t) \;=\; p_h(1) + p_h(2)t + p_h(3)t^2 \tag{3.3}$$

This effectively adds an amount of active control to the model, taking into account the

muscular activity present in real human walking. The coefficients of the quadratic-in-time moment comprise a vector, $\mathbf{p}_h$, that is treated as an additional unknown. Therefore the moment equation about point H is,

$$\Sigma \mathrm{M}_H \;=\; M_h(t) \;+\; \mathbf{r}_{HG_T} \times \mu_T \mathbf{g} \;+\; \mathbf{r}_{HG_S} \times \mu_S \mathbf{g} \tag{3.4}$$

$$=\; \mathbf{r}_{HG_T} \times \mu_T \mathbf{a}_T \;+\; \mathbf{r}_{HG_S} \times \mu_S \mathbf{a}_S \;+\; \dot{H}_T \;+\; \dot{H}_S$$

where the left hand side of the equation corresponds to the moments associated with the free body diagram and the right is the effective forces present in Figure 3.2. Additionally we model an internal moment at the knee that has the same form as (3.3),

$$M_k(t) \;=\; p_k(1) + p_k(2)t + p_k(3)t^2 \tag{3.5}$$

with the coefficients comprising a vector, $\mathbf{p}_k$, of unknowns. Therefore the moment equation about point K, considering only the shank resembles (3.4),

$$\Sigma \mathrm{M}_K \;=\; M_k(t) \;+\; \mathbf{r}_{KG_S} \times \mu_S \mathbf{g} \;=\; \mathbf{r}_{KG_S} \times \mu_S \mathbf{a}_S \;+\; \dot{H}_S \tag{3.6}$$

where the moment $M_k(t)$ is present in the free body diagram in Figure 3.3.

The vectors expressed in the three above moment equations are as follows,

$$\mathbf{r}_{CG_L} = (-\rho \sin\theta_L)\hat{\mathrm{i}} + (\rho \cos\theta_L)\hat{\mathrm{j}} \tag{3.7}$$

$$\mathbf{r}_{CH} = (-\ell \sin\theta_L)\hat{\mathrm{i}} + (\ell \cos\theta_L)\hat{\mathrm{j}} \tag{3.8}$$

$$\mathbf{r}_{CG_u} = \mathbf{r}_{CH} + (\eta \sin\theta_u)\hat{\mathrm{i}} + (\eta \cos\theta_u)\hat{\mathrm{j}} \tag{3.9}$$

$$\mathbf{r}_{CG_T} = \mathbf{r}_{CH} + (\tau \sin\theta_T)\hat{\mathrm{i}} - (\eta \cos\theta_T)\hat{\mathrm{j}} \tag{3.10}$$

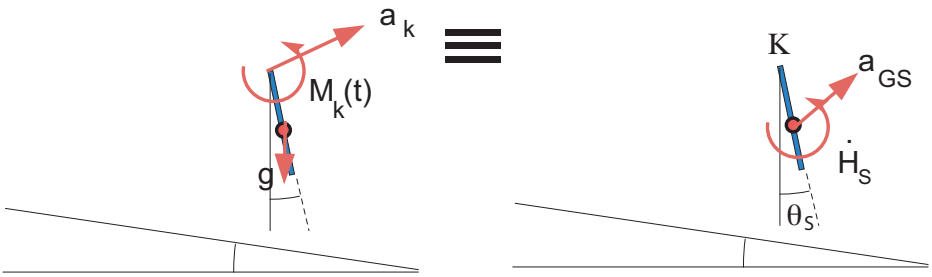

Figure 3.3: The free body and effective force diagrams are shown for the truncated kinetic model with only the shank present.

$$\mathbf{r}_{CG_S} = \mathbf{r}_{CH} + (d\sin\theta_T + \sigma\sin\theta_S)\hat{\mathrm{i}} - (d\cos\theta_T + \sigma\cos\theta_S)\hat{\mathrm{j}} \tag{3.11}$$

$$\mathbf{r}_{HG_T} = (\tau\sin\theta_T)\hat{\mathrm{i}} - (\tau\cos\theta_T)\hat{\mathrm{j}} \tag{3.12}$$

$$\mathbf{r}_{HG_S} = (d\sin\theta_T + \sigma\sin\theta_S)\hat{\mathrm{i}} - (d\cos\theta_T + \sigma\cos\theta_S)\hat{\mathrm{j}} \tag{3.13}$$

$$\mathbf{r}_{KG_S} = (\sigma\sin\theta_S)\hat{\mathrm{i}} - (\sigma\cos\theta_S)\hat{\mathrm{j}} \tag{3.14}$$

where $\hat{\mathrm{i}}$ and $\hat{\mathrm{j}}$ are the forward-horizontal and upward-vertical directional unit vectors associated with the inertial frame of reference defined. The 2-D assumption lends itself to the following relationships,

$$\omega_L = \dot{\theta}_L\hat{\mathrm{k}} \tag{3.15}$$

$$\omega_T = \dot{\theta}_T\hat{\mathrm{k}} \tag{3.16}$$

$$\omega_S = \dot{\theta}_S\hat{\mathrm{k}} \tag{3.17}$$

where the angular velocities, defined positive out-of-the-page. Centrifugal terms

are negated since the cross product of any of the ω vectors would result in zero ($\dot{\theta}_L\hat{\mathrm{k}} \times \dot{\theta}_T\hat{\mathrm{k}} = 0$).

Thus, the following kinematic relationships describe the effective accelerations,

$$\mathbf{a}_{G_L} = -(\rho\ddot{\theta}_L \cos\theta_L)\hat{\mathrm{i}} - (\rho\ddot{\theta}_L \sin\theta_L)\hat{\mathrm{j}} \tag{3.18}$$

$$\mathbf{a}_H = \mathbf{a}_{G_u} = -(\ell\ddot{\theta}_L \cos\theta_L)\hat{\mathrm{i}} - (\ell\ddot{\theta}_L \sin\theta_L)\hat{\mathrm{j}} \tag{3.19}$$

$$\mathbf{a}_{G_T} = \mathbf{a}_H + (\tau\ddot{\theta}_T \cos\theta_T)\hat{\mathrm{i}} + (\tau\ddot{\theta}_T \sin\theta_T)\hat{\mathrm{j}} \tag{3.20}$$

$$\mathbf{a}_K = \mathbf{a}_H + (d\ddot{\theta}_T \cos\theta_T)\hat{\mathrm{i}} + (d\ddot{\theta}_T \sin\theta_T)\hat{\mathrm{j}} \tag{3.21}$$

$$\mathbf{a}_{G_S} = \mathbf{a}_K + (\sigma\ddot{\theta}_S \cos\theta_S)\hat{\mathrm{i}} + (\sigma\ddot{\theta}_S \sin\theta_S)\hat{\mathrm{j}} \tag{3.22}$$

Due to the limbs being modeled as rigid bodies, the angular momentum derivative terms are therefore of the form, $\dot{H}_i = \mu_i k_i^2 \ddot{\theta}_i \hat{\mathrm{k}}$, with the subscript i standing in for the limb subscripts defined above.

Upon examining the moment equations, (3.2), (3.4) and (3.6), it is observed that all of the $\ddot{\theta}$ terms can be collected together. In doing so a 3x3 mass matrix, $\mathbf{A}'$, can be defined where,

$$\mathbf{A}' = \begin{bmatrix} A'_{11} & A'_{12} & A'_{13} \\ A'_{21} & A'_{22} & A'_{23} \\ A'_{31} & A'_{32} & A'_{33} \end{bmatrix} \tag{3.23}$$

with the first row corresponding to the expressions containing $\ddot{\theta_L}$, $\ddot{\theta_T}$ and $\ddot{\theta_S}$ respectively in (3.2), the second row containing similar expressions for (3.4), and the third

row for (3.6). After some simplification, these terms are written as follows:

$$A'_{11} = \mu_L(\rho^2 + k_L^2) + (\mu_u + \mu_T + \mu_S)\ell^2 + \mu_u \ell\eta\cos(\theta_L + \theta_u) \tag{3.24}$$

$$-\mu_T \ell\tau\cos(\theta_L - \theta_T) - \mu_S(d\cos(\theta_L - \theta_T) + \ell\sigma\cos(\theta_L - \theta_S))$$

$$A'_{12} = \mu_T(\tau^2 + k_T^2 - \ell\tau\cos(\theta_L - \theta_T)) \tag{3.25}$$

$$+\mu_S(d^2 - \ell d\cos(\theta_L - \theta_T) + d\sigma\cos(\theta_T - \theta_S))$$

$$A'_{13} = \mu_S(\sigma^2 + k_S^2 - \ell\sigma\cos(\theta_L - \theta_S) + d\sigma\cos(\theta_T - \theta_S)) \tag{3.26}$$

$$A'_{21} = -\mu_T \ell\tau\cos(\theta_L - \theta_T) - \mu_S\ell(d\cos(\theta_L - \theta_T) + \sigma\cos(\theta_L - \theta_S)) \tag{3.27}$$

$$A'_{22} = \mu_T(\tau^2 + k_T^2) + \mu_S(d^2 + d\sigma\cos(\theta_T - \theta_S)) \tag{3.28}$$

$$A'_{23} = \mu_S(\sigma^2 + k_S^2 + d\sigma\cos(\theta_T - \theta_S)) \tag{3.29}$$

$$A'_{31} = -\mu_S\ell\sigma\cos(\theta_L - \theta_S) \tag{3.30}$$

$$A'_{32} = \mu_S d\sigma\cos(\theta_T - \theta_S) \tag{3.31}$$

$$A'_{33} = \mu_S(\sigma^2 + k_S^2) \tag{3.32}$$

The remaining portions of the moment equations can also be collected. These "right hand sides" of the equations (3.2), (3.4) and (3.6) that do not contain angular acceleration terms can be expressed as functions f_1, f_2 and f_3. Thus, the equations of motion can be then written in state space form,

$$\mathbf{A}' \begin{bmatrix} \ddot{\theta}_L \\ \ddot{\theta}_T \\ \ddot{\theta}_S \end{bmatrix} = \begin{bmatrix} f_1(\mathbf{x}) \\ f_2(\mathbf{x}, t, \mathbf{p}_h) \\ f_3(\mathbf{x}, t, \mathbf{p}_k) \end{bmatrix} \tag{3.33}$$

Additionally, the unknown coefficients to the internal moments that have been defined are included with the unknown angles and angular velocities in the expressions on the right hand side since they are also unknown.

(3.33) can be augmented to accommodate the entire state vector from (3.1) in the following manner,

$$\begin{bmatrix} 1 & 0 & 0 & 0 & 0 & 0 \\ 0 & A'_{11} & 0 & A'_{12} & 0 & A'_{13} \\ 0 & 0 & 1 & 0 & 0 & 0 \\ 0 & A'_{21} & 0 & A'_{22} & 0 & A'_{23} \\ 0 & 0 & 0 & 0 & 1 & 0 \\ 0 & A'_{31} & 0 & A'_{32} & 0 & A'_{33} \end{bmatrix} \begin{bmatrix} \dot{\theta}_L \\ \ddot{\theta}_L \\ \dot{\theta}_T \\ \ddot{\theta}_T \\ \dot{\theta}_S \\ \ddot{\theta}_S \end{bmatrix} = \begin{bmatrix} \omega_L \\ f_1(\mathbf{x}) \\ \omega_T \\ f_2(\mathbf{x}, t, \mathbf{p}_h) \\ \omega_S \\ f_3(\mathbf{x}, t, \mathbf{p}_k) \end{bmatrix} \tag{3.34}$$

$$= \mathbf{A}\dot{\mathbf{x}} = \mathbf{f}(\mathbf{x}, t, \mathbf{p}_h, \mathbf{p}_k)$$

with the mass matrix entries, $\mathbf{A'_{ij}}$, encased in a new 6x6 matrix, $\mathbf{A}$. This is done because the matrix $\mathbf{A}$ can be inverted, thus,

$$\dot{\mathbf{x}} = \mathbf{A}^{-1}\mathbf{f}(\mathbf{x}, t, \mathbf{p}_h, \mathbf{p}_k) \tag{3.35}$$

becomes a compact form of the equations of motion that can be integrated once the initial conditions of $\mathbf{x}$ and moment coefficients $\mathbf{p}_h$ and $\mathbf{p}_k$ are determined. (3.35) therefore encapsulates the kinetic model.

Chapter 4

Step Size Estimation

As noted earlier, the objective of the work in this thesis is to develop a kinetic model of human gait to assist the calculation of an accurate, reliable navigation solution. *Step size* is one quantity that can be determined from the kinetic model. Therefore, estimates of step size can be used to form part of the navigation solution. This is because a step size estimate is a change-in-position measurement capable of being used in a dead reckoning solution. This chapter discusses how the kinetic model developed in Chapter 3 can be used to estimate step size.

4.1 Step Size vs. Stride Length

It is important to note that step size can be confused with a quantity typically called *stride length*. The stride length of an individual is defined as the distance traveled by the foot from the point where a foot leaves the ground at the beginning of a step to where it comes back into contact with the ground at the end of a step. In contrast, step size is the distance between the two feet of a person when both feet are in contact with the ground. Figure 2.1 illustrates this difference. The distinction between the two quantities is important because both can be determined via the states defined in

the kinetic model discussed in this thesis.

Step size is calculated using the following relation,

$$\hat{s}_k = -\ell \sin\theta_L(t_f) + d \sin\theta_T(t_f) + (\ell - d)\sin\theta_S(t_f) \tag{4.1}$$

which is nothing more than the geometric relationship between the angles at the end of the swinging of the free leg, at time $t = t_f$, and the limb lengths. The "hat" above a variable, in this case $\hat{s}_k$, denotes that the variable is an estimate. The subscript k is used to indicate the k^{th} step in a series of many steps. Thus, if the kinetic model defined is to be used to estimate step size, a time history of the angles of the limbs from some set point in time must be calculated. To do this, data from accelerometers will be used both as a means of detecting critical gait events and as inputs to the equations of motion.

In contrast, stride length is calculated using knowledge of the geometry of the legs at the beginning *and* end of the step. This means that stride length is the solution to (4.1) plus the solution to the same equation at some initial time, t_0. However, determining when a stride begins is somewhat ambiguous to determine, whereas the end is is not. As discussed previously, an accelerometer signal shows a spike at heel-strike, which signals the end of a stride. There is not an obvious acceleration cue for toe-off. Therefore, step size is easier to quantify and is the quantity that is studied in this thesis as a navigation aiding quantity.

4.2 Using Acceleration at the Ankle

In order to make the model behave in a way that is not passive, inputs are required to the equations of motion that, at least indirectly, take into account the forces and moments generated by the active contribution of the musculoskeletal system. One possible method that is discussed here is the use of accelerometers measuring specific force (acceleration including gravity) and rate gyros measuring angular rates placed at different points on the lower limbs. Signals from these sensors can provide a direct measure of the different forces and angular rates. More importantly they serve as a way of constraining the equations of motion to behave in a manner that is consistent with the sensors. The idea of using these sensors for this purpose is also the reason why they were employed as a means of examining the gait as discussed in Chapter 2 in order to build the foundation for the model discussed in Chapter 3.

The accelerometers worn at the ankle by the user will produce signals that capture the motion of the free leg shank. However there are two important issues to consider. First, accelerometers, being inertial sensors, capture the local acceleration due to gravity, which must be removed. Second, the orientation of the accelerometers with respect to an inertial frame of reference must be determined so that a rotation matrix can be calculated, enabling the gravity contribution to be removed.

The free body diagrams associated with deriving the kinetic model have inertial coordinate frames where the vertical, $\hat{\mathrm{j}}$, axis is antiparallel to the gravity vector. Thus, employing the angular definitions and 2-D assumption from before, the relationship between the accelerometer specific force outputs ($\tilde{a}_x$, $\tilde{a}_y$, $\tilde{a}_z$) and the acceleration

estimates ($\hat{a}_x$, $\hat{a}_y$, $\hat{a}_z$) is,

$$\hat{\mathbf{a}} = \begin{bmatrix} \hat{a}_x \\ \hat{a}_y \\ \hat{a}_z \end{bmatrix} = \begin{bmatrix} \cos\theta_S & \sin\theta_S & 0 \\ -\sin\theta_S & \cos\theta_S & 0 \\ 0 & 0 & 1 \end{bmatrix} \begin{bmatrix} \tilde{a}_x \\ \tilde{a}_y \\ \tilde{a}_z \end{bmatrix} - \begin{bmatrix} 0 \\ g \\ 0 \end{bmatrix} \tag{4.2}$$

In this equation the sensor orientation defined in Figure 2.8 is used. Here, g refers to the local gravitational acceleration in the same units as defined by the accelerometer signals (signified by the "tilde"). However, when used with the equations of motion, the net acceleration is scaled by dividing by the measured leg length, $\hat{\ell}$.

The second derivative of the step size equation works as the kinematic expression of the acceleration at the free leg ankle that can be used in place of one of the equations of motion. The expression,

$$\hat{a}_x = -\ell\ddot{\theta}_L\cos\theta_L + d\ddot{\theta}_T\cos\theta_T + (\ell-d)\ddot{\theta}_S\cos\theta_S + \ell\dot{\theta}_L^2\sin\theta_L - d\dot{\theta}_T^2\sin\theta_T - (\ell-d)\dot{\theta}_S^2\sin\theta_S \tag{4.3}$$

will work with accelerometer signals $\tilde{a}_x$ and $\tilde{a}_z$ as a replacement equation of motion. Additionally, the expression for the vertical acceleration,

$$\hat{a}_y = -\ell\ddot{\theta}_L\sin\theta_L + d\ddot{\theta}_T\sin\theta_T + (\ell-d)\ddot{\theta}_S\sin\theta_S - \ell\dot{\theta}_L^2\cos\theta_L + d\dot{\theta}_T^2\cos\theta_T + (\ell-d)\dot{\theta}_S^2\cos\theta_S \tag{4.4}$$

can be used.

Rearranging the equations to fit our state space form results in the following,

$$\begin{bmatrix} -\ell\cos\theta_L & d\cos\theta_T & (\ell-d)\cos\theta_S \\ -\ell\sin\theta_L & d\sin\theta_T & (\ell-d)\sin\theta_S \end{bmatrix} \begin{bmatrix} \ddot{\theta}_L \\ \ddot{\theta}_T \\ \ddot{\theta}_S \end{bmatrix} = \begin{bmatrix} \tilde{a}_x/\hat{\ell} - h_x(\mathbf{x}) \\ \tilde{a}_y/\hat{\ell} - h_y(\mathbf{x}) \end{bmatrix} \tag{4.5}$$

where the components h_x and h_y contain the angular velocity squared components from (4.3) and (4.4) respectively. The goal is to develop a method of using as few sensors as possible, then some manipulation of the equations to use only the $\tilde{a}_x$ accelerometer can be done. In this instance it can be shown that only a single accelerometer is needed to produce a virtual sensor that provides step size estimates.

By rearranging (4.2) in the following manner,

$$\begin{bmatrix} \tilde{a}_x \\ \tilde{a}_y \\ \tilde{a}_z \end{bmatrix} = \begin{bmatrix} \cos\theta_S & \sin\theta_S & 0 \\ -\sin\theta_S & \cos\theta_S & 0 \\ 0 & 0 & 1 \end{bmatrix}^{-1} \begin{bmatrix} \hat{a}_x \\ \hat{a}_y + g \\ \hat{a}_z \end{bmatrix} \hat{\ell} \tag{4.6}$$

the different accelerometer channels can be singled out. For instance, the equation for $\tilde{a}_x$ becomes,

$$\tilde{a}_x/\hat{\ell} = \hat{a}_x\cos\theta_S - (\hat{a}_y + g/\hat{\ell})\sin\theta_S \tag{4.7}$$

which makes use of both (4.3) and (4.4). As before, (4.7) is rearranged to fit the state space form,

$$\begin{bmatrix} -\ell\cos(\theta_L+\theta_S) & d\cos(\theta_T+\theta_S) & (\ell-d)\cos(2\theta_S) \end{bmatrix} \begin{bmatrix} \ddot{\theta}_L \\ \ddot{\theta}_T \\ \ddot{\theta}_S \end{bmatrix} = \tilde{a}_x/\hat{\ell} - h(\mathbf{x}) \tag{4.8}$$

where,

$$h(\mathbf{x}) = \ell\dot{\theta}_L^2 \sin(\theta_L + \theta_S) - d\dot{\theta}_T^2 \sin(\theta_T + \theta_S) - (\ell - d)\dot{\theta}_S^2 \sin(2\theta_S) - (g/\hat{\ell}) \sin\theta_S \quad (4.9)$$

contains the rest of the terms from (4.8) not associated with the angular accelerations.

Thus, the left hand terms of (4.8) can be substituted for $\mathbf{A'}_{31}$, $\mathbf{A'}_{32}$ and $\mathbf{A'}_{33}$ in (3.34) and the input, $\tilde{a}_x$, and remaining terms can be substituted for the corresponding right hand expression.

$$\begin{bmatrix} 1 & 0 & 0 & 0 & 0 & 0 \\ 0 & \mathbf{A'}_{11} & 0 & \mathbf{A'}_{12} & 0 & \mathbf{A'}_{13} \\ 0 & 0 & 1 & 0 & 0 & 0 \\ 0 & \mathbf{A'}_{21} & 0 & \mathbf{A'}_{22} & 0 & \mathbf{A'}_{23} \\ 0 & 0 & 0 & 0 & 1 & 0 \\ 0 & -\ell\cos(\theta_L + \theta_S) & 0 & d\cos(\theta_T + \theta_S) & 0 & (\ell - d)\cos(2\theta_S) \end{bmatrix} \begin{bmatrix} \dot{\theta}_L \\ \ddot{\theta}_L \\ \dot{\theta}_T \\ \ddot{\theta}_T \\ \dot{\theta}_S \\ \ddot{\theta}_S \end{bmatrix} = \begin{bmatrix} \omega_L \\ f_1(\mathbf{x}) \\ \omega_T \\ f_2(\mathbf{x}, t, \mathbf{p}_h) \\ \omega_S \\ \tilde{a}_x - h(\mathbf{x}) \end{bmatrix}$$

$$= \mathbf{A}\dot{\mathbf{x}} = \mathbf{f}(\mathbf{x}, t, \mathbf{p}_h, \tilde{a}_x) \quad (4.10)$$

The compact form of the equations of motion with the accelerometer signal injected therefore becomes,

$$\dot{\mathbf{x}} = \mathbf{A}^{-1}\mathbf{f}(\mathbf{x}, t, \mathbf{p}_h, \tilde{a}_x) = \mathbf{g}(\mathbf{x}, t, \mathbf{p}_h, \tilde{a}_x) \quad (4.11)$$

It is important to note, that with the way the input accelerometer signal is included in the equations of motion, there is no need to solve for the moment coefficients modeled at the knee, $\mathbf{p}_k$. This is essentially equivalent to using a measured acceleration value to solve for this moment and by extension go about solving for the rest of the unknowns in the equations of motion. Similarly, using (4.5) would replace both moments and require two accelerometer channels, thus making the states, $\mathbf{x}$, the only unknowns.

The rest of this thesis will consider the single accelerometer method of determining step size. Assessment of the multiple accelerometer approach is potential future work.

4.3 Detecting the Swing

To employ any sensor measurements in concert with the equations of motion a swing detection algorithm is required. This algorithm processes the acceleration data streaming in and "picks out" the sections of it that represent the swing portion of the gait cycle. The swing is the portion of the complete gait cycle that we are concerned with because it contains all of the "stride creating" motion (the rest of the gait cycle can be thought of as being "stride supporting"). To do this, a set of acceleration data is either manually assessed and segmented or sent through a search algorithm that uses mathematical relationships to identify the occurrence of key signature events specific to the swing phase pattern in the data (e.g. a peak corresponding to toe-off). The process effectively takes a time history of accelerometer data and distills it down into a set of swing phase data segments that individually consist of several data points over an approximate duration of a third of a second and are separated in time from the other data segments.

Figure 4.1 displays the segment of interest in black with the rest of the accelerometer signal in blue. Additionally, stick figures representing the legs of the walker modeled display still-poses of the beginning and end of the highlighted segment as captured by the Vicon motion capture system. This is the portion of the data that the equations of motion is integrated over.

The algorithm used keys off two threshold values that are experimentally determined

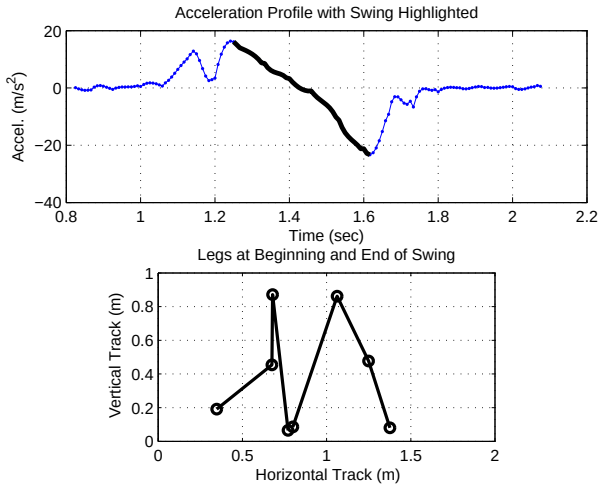

Figure 4.1: The top figure highlights the swing portion of the acceleration signal capturing the gait cycle at the ankle. The bottom figure displays still wire-frame images of the model at the beginning and end of the highlighted portion in the top figure. Data was acquired via the Vicon motion capture system.

in i.e. a calibration test where IMU data is captured at the ankle of a person intending to use the navigation system. The first threshold is a minimum acceleration that must be seen in order to identify the duel peak formation in Figure 4.1. The second threshold is a maximum acceleration value used to identify the end of the swing. Depending on a person's size, the magnitudes of the accelerations at the beginning and end of the swing will change and it is important to select thresholds that won't detect smaller peaks and troughs that might be anomalies or different parts of the gait profile. Additional experiments with several subjects of varying height could potentially lead to an empirical relationship between e.g. a person's height and these threshold values. That determination is a potential future study.

4.4 Solving the Equations of Motion

The process of estimating the step size of an individual during an instance of the gait cycle is challenging because solving the equations of motion is not trivial. Essentially, the goal in solving the equations is to arrive at a set of initial conditions for $\mathbf{x}$ and moment coefficients $\mathbf{p}_h$, based on which the equations of motion will be integrated. Ultimately, once the equations are integrated over the duration of the swing, the step size can be determined using the estimated angles at the final time of the integration.

There are three equations for three unknown initial angles, three unknown initial angular velocities and three moment parameters. This means that six additional equations would be required in order to determine a closed form solution. However, there are no apparent expressions that can provide this. Therefore the approach taken is a numerical optimization approach using functional minimization. In order to numerically determine the unknown quantities, several constraints are defined. These constraints are defined as *step boundary conditions* because they represent quantities that vary little to not at all from step to step.

4.4.1 Step Boundary Conditions

As noted in Chapter 2, the gait profile is similar across individuals. This suggests that certain key features in a person's gait can be used for the purposes of determining the unknown parameters in the equations of motion. A study of the time histories of the angles θ_L, θ_T, and θ_S and their derivatives for a walking person reveals some largely invariant quantities that may be expressed as functions of these angles and their derivatives at specific times during the step. Specifically, many of these quantities can be identified at the beginning or end of a step, therefore making

them boundary conditions. In addition, these boundary conditions can be estimated by evaluating many steps by a particular individual i.e. in a model calibration task.

Six such quantities are identified. All are assessed at the final time, i.e. at heel-strike. These quantities are defined as a vector, ψ, where,

$$\psi_1 = \ell \cos\theta_L(t_f) - d\cos\theta_T(t_f) + (\ell - d)\cos\theta_S(t_f) \tag{4.12}$$

$$\psi_2 = \theta_L + \theta_T \tag{4.13}$$

$$\psi_3 = \theta_T - \theta_S \tag{4.14}$$

$$\psi_4 = \dot{\theta}_L \tag{4.15}$$

$$\psi_5 = \dot{\theta}_T \tag{4.16}$$

$$\psi_6 = \dot{\theta}_S \tag{4.17}$$

A qualitative explanation of each of the above boundary conditions is as follows:

- ψ_1: the height above the ground of the heel at heel-strike which obviously should be zero
- ψ_2: the difference in the magnitudes of the thigh angle and the stance leg angle (note that the stance leg angle is negative at heel strike)
- ψ_3: the difference in the the thigh angle and the stance leg angle
- ψ_4: angular velocity of the stance leg
- ψ_5: angular velocity of the thigh
- ψ_6: angular velocity of the shank

Parameter	Mean	Std. Dev.
ψ_1 (m)	-0.025	0.035
ψ_2 (rad)	0.21	0.06
ψ_3 (rad)	0.19	0.13

Table 4.1: Mean and standard deviation of certain step boundary conditions.

The time at the end of the swing that has been extracted from the acceleration profile is defined as $t = t_f$. At this final time, the step boundary conditions can effectively be solved for using an expression defined as,

$$\psi(\mathbf{x}_f, t_f) = \begin{bmatrix} \psi_1 & \psi_2 & \psi_3 & \psi_4 & \psi_5 & \psi_6 \end{bmatrix}^T \tag{4.18}$$

or the process of assembling (4.12-17) using,

$$\mathbf{x}_f = \hat{\mathbf{x}}_0 + \int_{t_0}^{t_f} \dot{\mathbf{x}} dt \tag{4.19}$$

or the states at the end of the swing given some estimated initial conditions, $\hat{\mathbf{x}}_0$.

By definition, these boundary conditions are singled out because their variation between similar steps is relatively small. Table 4.1 displays some statistical quantities related to the first three boundary conditions for a particular individual. The means and standard deviations are calculated using Vicon motion capture data from approximately 20 steps.

It is assumed that the means of the final three boundary conditions are zero. This is done because the angular velocities of the three limbs is observed to be near zero once the heel-strike occurs and both feet are briefly in contact with the ground.

4.5 Generating Initial Conditions

The initial angle conditions are not numerically determined. Instead an educated guess is provided in one of two ways. First, in a stand alone mode where the user is wearing a single, forward-facing accelerometer on just one leg the initial angles are assumed to be the angles associated with a completely symmetric step of average step size. Essentially a person's average step size, $\bar{s}$, is determined by observing their natural gait and the initial angles are determined by,

$$\hat{\theta}_{0_L} = -\hat{\theta}_{0_T} = -\hat{\theta}_{0_S} = \sin^{-1}\left(\frac{\bar{s}}{2\hat{\ell}}\right) \tag{4.20}$$

Second, in the case where an accelerometer is worn on both feet, thus allowing step size to independently be estimated by each leg, determine the initial angles for the next step via the final angles of the step that was completed by the other leg.

To solve for the initial angular velocities and moment parameters, $\mathbf{p}_h$, a scalar quantity is defined,

$$\chi = (\psi - \bar{\psi})^T \mathbf{R} (\psi - \bar{\psi}) \tag{4.21}$$

where χ, the optimization cost function, is the result of a weighted inner product with the difference between the numerically calculated ψ and observed average boundary conditions, $\bar{\psi}$. A six by six diagonal weighting matrix,

$$\mathbf{R} = \begin{bmatrix} \sigma_{\psi_1} & 0 & 0 & 0 & 0 & 0 \\ 0 & \sigma_{\psi_2} & 0 & 0 & 0 & 0 \\ 0 & 0 & \sigma_{\psi_3} & 0 & 0 & 0 \\ 0 & 0 & 0 & \sigma_{\psi_4} & 0 & 0 \\ 0 & 0 & 0 & 0 & \sigma_{\psi_5} & 0 \\ 0 & 0 & 0 & 0 & 0 & \sigma_{\psi_6} \end{bmatrix} \tag{4.22}$$

is composed of hand tuned weights on the diagonal that essentially assign one or more invariants as being more important or reliable compared to others. In practice, ψ_1 is considered the most significant boundary condition, since by definition it will force the foot back to level ground.

The scalar, χ, is then driven to zero in a functional minimization routine. In the work reported in this thesis the MATLAB optimization function *fminsearch* was used. This is achieved by the routine iteratively determining a combination of initial angular velocities and moment parameters that satisfy the conditions of the step defined by the stride invariants and input accelerometer signal. To decrease the locus of possible solutions and shorten computation time, guesses of the initial angular velocities and moment parameters are used that are assigned based on quantities from previous steps.

The resulting numerical solution is used with (4.19) to integrate the equations of motion a final time. The three limb angles at $t = t_f$ are then used in (4.1) to calculate the step size estimate.

Chapter 5

Algorithm Validation

To assess the performance of kinetic model in the role of determining stride length data from a variety of experiments was analyzed. Three different experimental setups were used. First, laboratory data from various volunteer individuals comprising a large set of "normal gait data" obtained using the Vicon system was available for analysis at Gillette Children's Hospital in St. Paul, Minnesota. This data contains position history of different points on the human body for several individuals walking a few steps of different sizes and speeds. Second, data was taken at the ankle using the MIDG II with the individual walking on a longer predesigned indoor course. Finally, data obtained from a test individual walking in an outdoor environment was analyzed. The outdoor experiments allowed us to compare the stride length estimation position error growth versus a naive GPS assisted dead reckoning positioning approach.

5.1 Motion Capture Laboratory Analysis

The motion capture data from the lab at Gillette Children's Hospital contained inertial position history data of 15 markers placed at specific points on the body of

volunteer individuals. The most significant points where these markers were placed for our analysis were the protruding hip bone, or anterior superior illiac spine just above the left and right hip joints, the outward part of the femur at the knee joints (lateral femoral epicondyle) and at the ankles (lateral malleolus). In addition to the position histories of those and other points on the body information such as joint center position histories and indices of events such as toe-off and heel-strike were provided in addition to other essential information such as limb length and mass. The coordinate axes of the position data are oriented in such a way that the forward, or x-direction is the direction of travel of the individual while the y and z directions are defined as the lateral and vertical directions respectively.

The motion capture data was used to analyze how the results from the stride length estimation procedure vary from reality. To do this, numerically synthesized accelerometer measurements were calculated from the position histories of the markers at the hip, knee and ankle of each leg during each data run. These simulated accelerometer measurements were used as the input to the equations of motion instead of the MIDG accelerometer. Synthesized accelerometer data was used because the motion capture data was collected prior to the start of this research. Figure Figure 5.1 displays plots of the angular histories as determined via the Vicon measurements versus the estimated angular histories from the equations of motion.

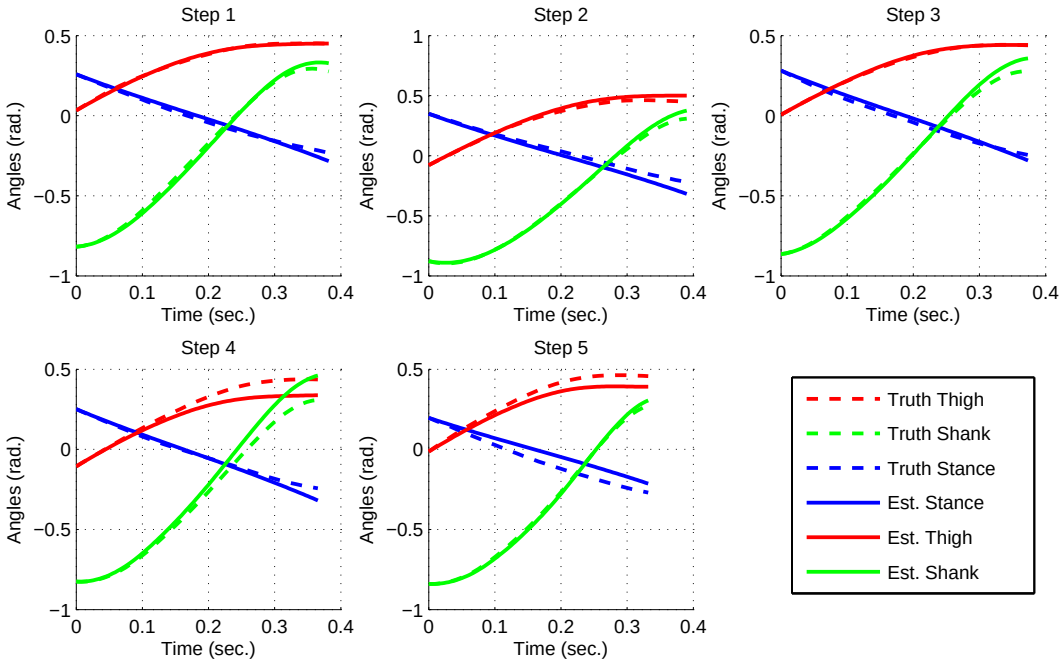

Figure 5.1: The synthesized angular histories tracking the left leg for five consecutive steps is plotted (dashed lines) for each of the three limbs defined are plotted with the estimated angular histories resulting from the equations of motion.

5.2 Indoor Test with Accelerometer Data

An indoor walking course was set up on a tiled floor, where a test subject would walk on a sequence of tape markings coinciding with tile cracks. These markings were separated at distances of either 24 or 36 inches for reasons of convenience with the 12 inch tile size and because those step sizes are reasonable for varying height adults. The distance between tape markings changed size on an inconsistent basis as they were laid in a straight-line down a hallway section. In conducting the test, a test subject walked on a set of tape marks down the hallway with a total distance of 120 feet. The subject then turned around and walked on a different set of tape marks with a different sequence of altering step sizes back to the original starting position. In addition, the subject was instructed to have the arch of their foot come into contact with the tape markings for easier, more accurate referencing. That instruction gives added faith to the results traced in Figure Figure 5.2, where the estimator correctly guesses the step size in-situ.

Figure Figure 5.3 is a plot of the dead reckoning solution to what is presented in Figure Figure 5.2. The alternating 24 and 36 inch step estimates are summed and compared graphically to where the end of the outbound leg of the course should be. At this point, the dead reckoning solution is short by 0.259 meters. The inbound leg is then superimposed from the calculated end of the outbound leg. The round trip error is calculated to be approximately 0.079 meters.

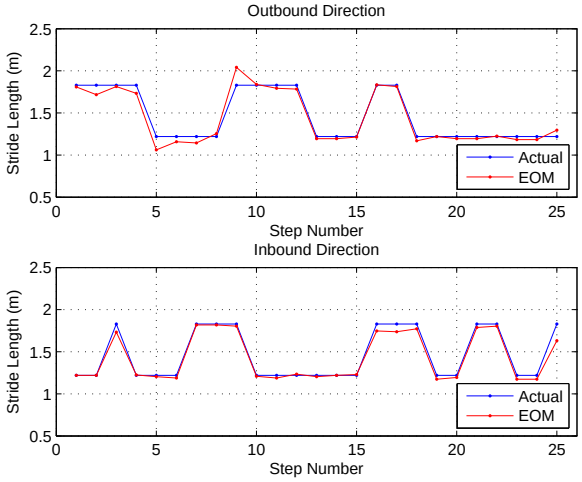

Figure 5.2: Stride length estimates are compared with truth references in the form of tape marking guides when step size is intentionally toggled between 24 and 36 inch (.61 and .91 meter) step sizes. The 244 foot (74.37 meter) round trip is broken into 122 foot (37.19 meter) outbound and inbound segments.

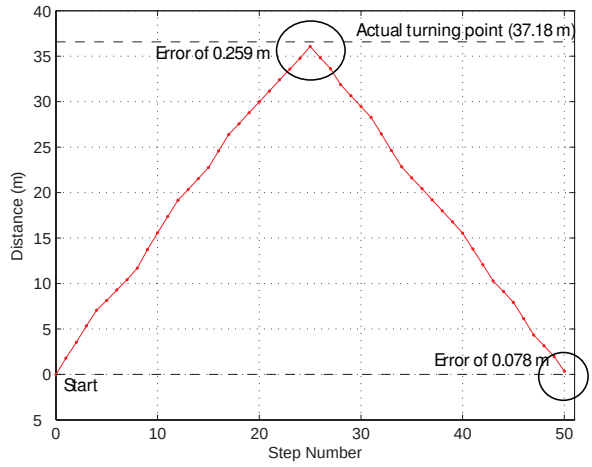

Figure 5.3: The dead reckoning position solution using the estimates from Figure Figure 5.2 is calculated as outbound and inbound distance from the starting position.

5.3 Outdoor Test with Accelerometer Data

For a basis of comparison against another common personal dead reckoning navigation method, a large set of walking data was collected walking in a relatively open space on the edge of the University of Minnesota Minneapolis East Bank Campus. Here, natural walking with deliberate and incidental pace and stride changes was done in the midst of pedestrian traffic and other obstacles such as light posts, trees, and surface terrain changes. Figure 5.4 is a display of this walking track overlayed on a map.

In addition to collecting acceleration data at the ankle with the MIDG II, the built-in GPS receiver gave position tracking data that was used with what we call a naive step size estimator. This approach to personal dead reckoning is similar to the shoe-mounted sensor and step counting algorithms discussed in [26, 27]. A more detailed description of this naive step counting method is given next.

5.3.1 Step Counting Comparison

While step counting is nothing new, its relative simplicity has made it commercially successful such as with the Nike + iPod Sport Kit designed for runners [28]. The idea is to count steps and propagate position history forward in time using a constant, predetermined step size. This approach is referred to in this thesis as the *naive approach* because of its simple nature. The term naive is used because this approach assumes step sizes are constant over some time interval. All that is required is some signal to let the navigator know a step has occurred, and with the assumed constant step size the position is propagated forward in-situ. In order to calculate a 2-D solution, heading is also needed. This can be supplied by a compass (magnetometers) or

Figure 5.4: The trace of the outdoor walking course is drawn on a map that is copyright the University of Minnesota Board of Regents. The region outlined by the yellow box is the section of data specifically analyzed using the stride length estimation algorithm because on the day of the test, people and obstacles were present in this region causing less consistent step sizes.

calculated from GPS velocity.

In our implementation of the naive step size estimator, we used GPS velocity at 5Hz to calculate heading. To calculate step size in the naive approach, the GPS points coinciding with the previous 20 steps at any given instant were used. More specifically, the GPS position solution is used to calculate the distance traveled. This is divided by 20 to estimate the user's step size. This estimate was continuously refined over a moving 20 step window so that the current step size was based on GPS data from the 20 previous steps. The same data was used to determine the GPS-determined heading at each step instant. Using this time history of naive step size estimates and heading, a dead reckoning solution was calculated. Next, we used the kinetic model developed in this paper to estimate step size and combine this with the GPS-determined heading to mechanize a personal dead reckoning system.

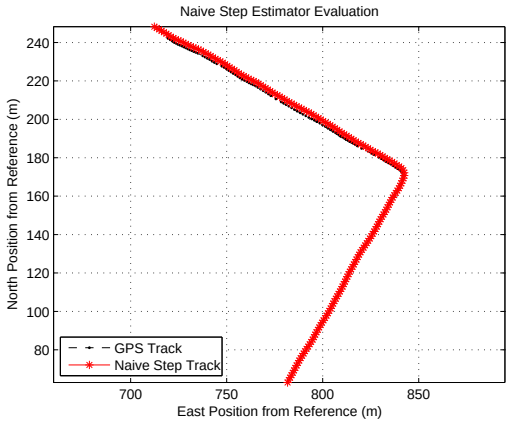

Figure 5.5: The GPS track and naive DR solution are plotted for the two minute section highlighted in Figure Figure 5.4.

In the two minute section of the outdoor data set highlighted in Figure 5.4, Figure 5.5, and Figure 5.6, the error appears to drift considerably with the naive approach. This is expected since the time histories of the GPS track and step occurrences are required in the naive stride length estimation. The error in Figure Figure 5.6 is approximately 6% of the distance traveled during the two minute walk.

The use of the kinetic model for stride length estimation demonstrated a tempered error growth rate in the indoor validation experiment. This also is true with the outdoor experiment. Figure 5.7 displays the same two minute window from Figure 5.5. The same set of GPS data shows varying error growth rates instead of a drift. This is demonstrated by the changing slope of the EOM position track in Figure 5.7. Whereas the naive approach was off by 9.3 meters after two minutes the kinetic model approach demonstrated a 0.8 meter error.

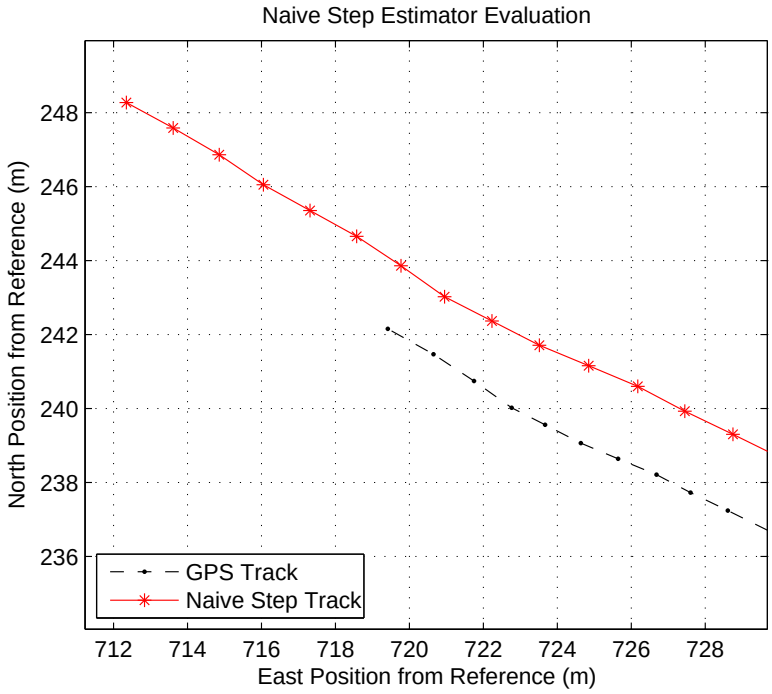

Figure 5.6: Zooming in on the previous figure displays the naive approach has drifted 9.3 metersaway from the GPS track (approx. 6% of distance traveled).

[!]

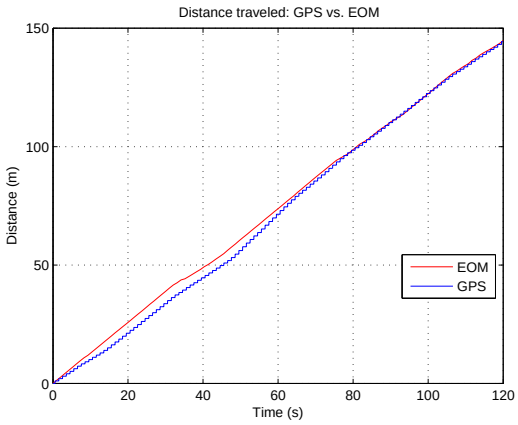

Figure 5.7: The dead reckoning position solution using stride length estimates calculated with the kinetic model areplotted against the GPS position trace over the same two minute window as Figure Figure 5.4.

Chapter 6

Sensitivity Analysis

Due to the multilayered, complex nature of the problem, any errors associated with limb length estimation, sensor bias and noise, integration, modeling, etc. are buried ambiguously into the all of the states. As such, analyzing the accuracy of the stride length estimates cannot be done in a way that provides a closed form numerical solution to the state errors and their covariances at the final time of each stride. It is still desired to have some means of qualitatively, if not quantitatively, assessing how well the kinetic model works at producing stride length estimates. Furthermore, it is desired to know what sources of error contribute more significantly to an erroneous solution as compared to others. Thus, Monte Carlo simulations are employed in different ways to assess how the model is sensitive different errors that can degrade the stride length solution.

A Monte Carlo simulation is one in which certain pre-calculation parameters are randomly varied by a small, but significant amount many thousands or millions of times, so that the result of employing an algorithm with the perturbed parameters is a perturbed solution. Performing this analysis with many data points can provide an idea of how different errors impact a particular solution. For the Monte Carlo simulations discussed below, data from three individuals was manipulated in a variety of ways

and step size was calculated. The step size estimates are normalized in such a way as to compare the data together as one set. There are a total of 250,000 data points for each simulation, capturing twenty-five steps from the three individuals.

6.1 Sensitivity to Initial Condition Errors

A critical component of estimating step size in the manner presented in this thesis is the determination of initial conditions. As discussed in Chapter 4, the process of determining the initial conditions is not trivial. As such, we expect some of the error in the step size estimate to come from bad initial conditions.

The initial angles and initial angular velocities impact the model performance in a slightly different manner. The model depends heavily on the angular velocities, both for calculating the angular accelerations and for the determination of the limb angles via integration. Thus, we analyze variations in each of them separately.

First, we randomly vary the initial conditions before integrating the equations of motion. This is done using the relation

$$\hat{\mathbf{x}}_0 \;=\; \mathbf{x}_0 + w_0 \tag{6.1}$$

where w_0 is a vector of Gaussian zero-mean white noise,

$$w_0 \sim N(0, Q_0) \tag{6.2}$$

with covariance Q_0 that we can tune at the beginning of the simulation. Each time the simulation runs, it is perturbing the initial conditions by a random amount, w_0.

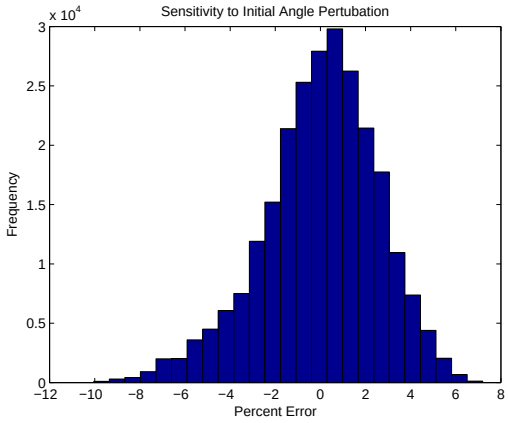

Figure 6.1: A histogram of the normalized step size errors generated by perturbing the initial angle conditions of estimation process in a Monte Carlo simulation.

However, we only employ the perturbed initial conditions for the angles or the angular velocities in separate instances; not at the same time.

Figure Figure 6.1 is a histogram of the normalized errors of perturbing the initial angle conditions. The errors are normalized by

$$e = \frac{\hat{s} - \bar{s}}{\bar{s}} \tag{6.3}$$

subtracting the estimated step size, $\hat{s}$, from the truth reference, $\bar{s}$, and then divided by the true step size value. In doing so the histogram in Figure 6.1 attempts to capture the error probabilistic history from errors in the initial conditions over different stride lengths. Q_0 entries were defined as varying by a standard deviation of 0.1 radians. It is shown that perturbing the initial angles in this manner can produce significantly large errors. The distribution of errors is interestingly skewed toward positive, or long stride estimates.

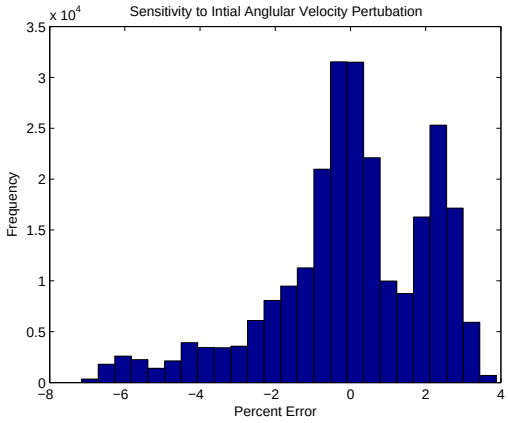

Figure 6.2: A histogram of the normalized step size errors generated by perturbing the initial angular velocity conditions of estimation process in a Monte Carlo simulation.

Figure 6.2 displays the step size estimates when perturbing the initial angular velocities instead of the initial angles. For this simulation, the angular velocities were varied using a standard deviation of 0.1 radians per second when generating normally distributed perturbations. Interestingly, the worst case error displayed is significantly less than that seen when varying the initial angles. However, two distinct peaks seen in Figure 6.2 potentially suggest that perturbing one of the angular velocities more significantly than the others can generally produce a longer, more erroneous step size estimate. Detailed correlation studies may be of interest in future work to determine if this is in fact the case.

6.2 Sensitivity to Model Parameter Errors

If the inertial parameters that are used in the equations of motion are defined as a vector ζ,

$$\zeta = \begin{bmatrix} \ell & d & \mu_T & \delta & k_L & k_T & \dots \end{bmatrix} \tag{6.4}$$

that contains variables such as leg length, ℓ, thigh length, d, center of mass of shank from knee, μ_T, thigh center of mass from hip, δ, stance leg radius of gyration, k_L, thigh radius of gyration, k_T, etc. We can randomly vary them using the relation

$$\hat{\zeta} = \zeta + w_\zeta \tag{6.5}$$

that adds Gaussian zero-mean white noise vector, w_ζ,

$$w_\zeta \sim N(0, Q_\zeta) \tag{6.6}$$

with covariance values Q_ζ. The variances of Q_ζ are all set at ten percent of the values they correspond to. This provides a simulation for errors in the way we have modeled the human gait dynamics.

However, since step size estimates are directly dependent on the limb lengths, we choose to analyze perturbations of those parameters separately from the rest of the mass and moment of inertia parameters. Figure 6.3 displays the results when perturbing only the limb lengths. Again, this form of error seems to contribute less of an impact as the initial angles. The double peak is once again present, suggesting that the longest limb, the stance leg, is important to model accurately. This reflects a key assumption made in earlier where we assume a perfectly straight stance leg that does not have a knee.

Figure 6.4 depicts a histogram of the normalized step size error distribution resulting from the Monte Carlo simulation varying the mass and moment of inertia parameters. The distribution again shows multiple peaks, and errors that seem to be smaller than the initial angle perturbations. More research needs to be done to investigate the roles of modeling different mass and inertia parameters has on step size estimate

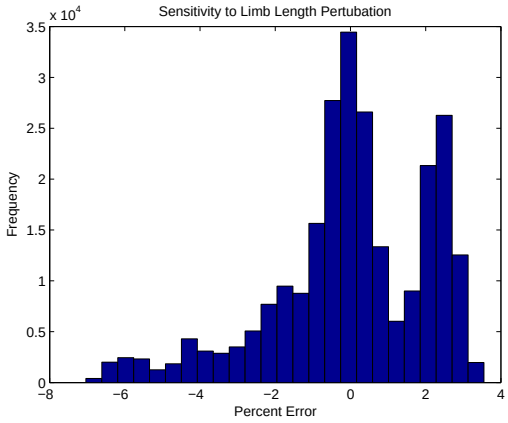

Figure 6.3: A histogram of the normalized step size errors generated by perturbing the limb lengths used in the kinetic model in a Monte Carlo simulation.

errors.

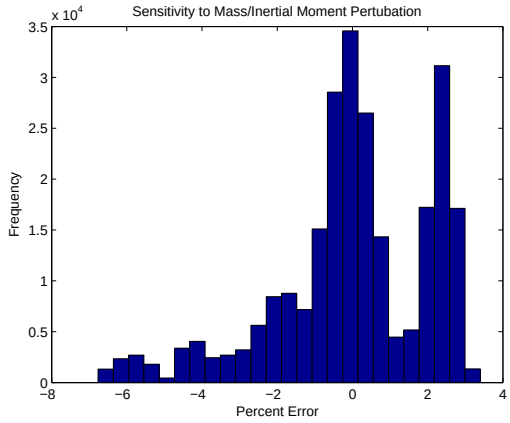

Figure 6.4: A histogram of the normalized step size errors generated by perturbing the mass and moment of inertia parameters used in the kinetic model in a Monte Carlo simulation.

6.3 Sensitivity to Sensor Errors

Adding additional noise onto accelerometer signals used in the step size estimation process, errors are simulated on that sensor itself. Injecting noise in this way attempts to study the impact of errors contributed on the measurement level. Additionally, since accelerometer measurements are the input to the equations of motion, errors in the accelerometer signal are errors that are not associated with the modeling process or determination of initial conditions, i.e. the errors discussed in the previous two sections. Thus, sensor error contributions are unique to the hardware used. Studying sensor based errors in the step size estimation process can provide insight into the quality of sensors needed to produce accurate step size estimates.

The relation,

$$\hat{a}^b_{ib}|_x = a^b_{ib}|_x + v_{a_x} \tag{6.7}$$

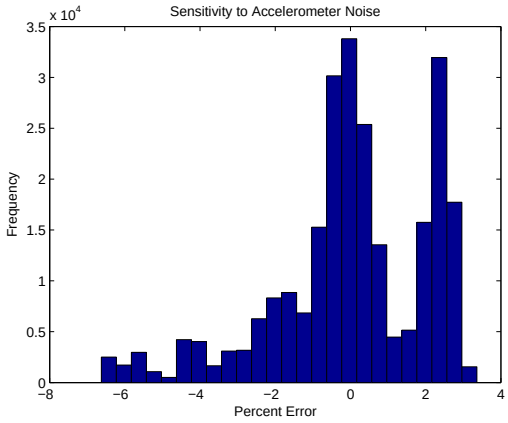

Figure 6.5: A histogram of the normalized step size errors generated by perturbing the acceleration measurements used with the kinetic model to generate stride length estimates in a Monte Carlo simulation.

performs the introduction of errors by adding a Gaussian zero-mean noise vector

$$v_{a_x} \sim N(0, R_{a_x}) \tag{6.8}$$

where the covariance R_{a_x} is on the order of 1 meter per second squared.

Perturbing the measurements as such produces the histogram in Figure 6.5 that has a mean normalized stride length error of 1.6%. However, the probability distribution depicted in Figure 6.5 also displays multiple peaks not unlike what was observed previously. This may be due to the acceleration measurements being tied to the calculation of the initial conditions.

The results indicate that poor quality commercial-off-the-shelf accelerometers are acceptable for use. Erroneous initial conditions or poor estimates of inertial parameters used by the kinetic model to estimate step size seem to contribute larger net errors. Thus, improving the kinetic model to produce better step size estimates is necessary

before considering how better sensors can improve performance.

Chapter 7

Conclusions

A kinetic model for human gait in planar walking was developed and analyzed for personal navigation. This kinetic model consists of the equations of motion for normal human gait. The equations of motion in conjunction with an accelerometer measurement input created a virtual sensor for estimating stride length and stride time. Due to the second order nature of the equations of motion, the ability to estimate stride length is dependent on initial conditions and internal joint moment parameters which we generate based on quantities defined as stride invariants. Natural variability in the human gait from step to step lends itself to variability in the stride invariants and thus errors in the stride length estimate. In addition, sensor bias and noise in the accelerometer and equation of motion parameter calculation errors can also contribute to errors that degrade the stride length estimates.

In an indoor experiment, the equations of motion were used with a step detection algorithm to estimate changing step sizes that were truth referenced using tape marks. The stride lengths were correctly estimated and the position error growth associated with tracking the user's position moving down the hallway appeared to have been arrested.

In an outdoor experiment, the error growth during a two minute window was compared to the error growth using a naive step counting dead reckoning approach. The significant drift in stride length estimation error with the naive approach caused a significant deviation in position estimation from the GPS track while the kinetic model approach yielded a smaller error. The error for the step counting (naive) approach was 9.3 meters while the model yields an error of 0.8 meters. In percent of distance traveled it is a decrease from 6% to less than 1% error over the two minute stretch.

Bibliography

[1] Hide, C., T. Botterill and M. Andreotti. "Vision-Aided IMU for Pedestrian Navigation." *Proc. ION GNSS*, Portland, OR, September 2010.

[2] DROID X Specifications.

[3] McCroskey, R., et al. "GLANSER - An Emergency Responder Locator System (ERLS) for Indoor and GPS-Denied Applications." *Proc. ION GNSS*, Portland, OR, September 2010.

[4] Soehren, W., and W. Hawkinson. "A Prototype Personal Navigation System." *Proc. IEEE/ION PLANS*, San Diego, CA, April 2006, pp. 539-546.

[5] Molina, P., et al. "Non-Conventional INS/GNSS Integration for Qualitative Motion Analysis in Caregiving Applications." *Proc. ION GNSS*, Portland, OR, September 2010.

[6] Gafurov, D., et al. "Biometric Gait Authentication Using an Accelerometer Sensor." *Journal of Computers*, Vol. 1, No. 7, October/November 2006. pp. 51-59.

[7] Boyd, J. and J. Little. "Biometric Gait Recognition." *LNCS: Advanced Studies in Biometrics*. Springer Berlin / Heidelberg, Volume 3161, 2005, pp. 19-42.

[8] Groves, Paul D. *Principles of GNSS, Inertial, and Multisensor Integrated Navigation Systems*. Artech House (Boston), 2008, pp. 335-337, 437-444.

[9] Du, G. et al. "A Flexible Low-Cost Time Synchronizer for GNSS/INS Integration." *Proc. ION GNSS*, Portland, OR, September 2010.

[10] Misra, P. and P. Enge. *Global Positioning System Signals, Measurements and Performance*. Ganga-Jamuna Press, 2001.

[11] Foxlin, Eric. "Pedestrian Tracking with Shoe-Mounted Inertial Sensors." *IEEE Computer Graphics and Applications*, Vol. 25, 06, November/December December 2005, pp. 38-46.

[12] Whittle, M. *Gait Analysis: An Introduction*. Oxford: Butterworth-Heinemann, 1996.

[13] Moafipoor, Shahram, Dorota A. Grejner-Brzezinska, and Charles K. Toth. "A Fuzzy Dead Reckoning Algorithm for a Personal Navigator." *Journal of The Institute of Navigation*, Vol. 55, No. 4, pp. 241-253.

[14] Frank, K., et al. "Reliable Real-Time Recognition of Motion Related Human Activities using MEMS Inertial Sensors." *Proc. ION GNSS*, Portland, OR, September 2010.

[15] van Deursen, Robert W.M., Timothy W. Flynn, et al. "Does a Single Control Mechanism Exist for Both Forward and Backward Walking?" *Elsevier Gait and Posture* 7, 1998, pp. 214-224.

[16] Pantazis, Ioannis. M.S. Thesis, Electrical Engineering, "Tracking Human Walking Using MARG Sensors." Naval Postgraduate School. June 2005.

[17] Pogemiller, J. A simple passive dynamic walker. *http* : $//www.youtube.com/watch?v = 0tCZQD0l_qQ$. University of Minnesota-Twin Cities, last updated December 2008.

[18] A spring-kneed passive walker. *http : //www.youtube.com/watch?v = CK8IFEGmiKY*. Nagoya Inst. of Tech., last updated June 2005.

[19] McGeer, T. "Passive Dynamic Walking." *Internation Journal of Robotics Research*, Res. 9, 1988, pp. 62-82.

[20] Pearsall, D.J. and P. Costigan. "The Effect of Segment Parameter Error on Gait Analysis Results." *Elsevier Gait and Posture* 9, 1999, pp. 173-183.

[21] Microbotics, Inc. The MIDG II INS/GPS. *http : //www.microboticsinc.com/ins$_g$ps.html*. Last accessed September 2010.

[22] Vicon Motion Systems, Vicon MX information website. *http : //www.vicon.com/products/viconmx.html*. Last updated August 2010.

[23] Clauser, C.E., McConville, J.P., and J.W. Young. "Weight, Volume, and Center of Mass of Segments of the Body." *Aerospace Medical Research Laboratories*, Ohio, 1969.

[24] Croce, Ugo Della, Patrick O. Riley, et al. "A Refined View of the Determinants of Gait." *Elsevier Gait and Posture* 14, 2001, pp. 79-84.

[25] Ginsberg, J. *Engineering Dynamics*. Cambridge University Press (New York), 2008, pp. 296-390.

[26] Groves, Paul D., et al. "Inertial Navigation Versus Pedestrian Dead Reckoning: Optimizing the Integration." *Proc. ION GNSS*, September 2007, Fort Worth TX, pp. 2043-2055.

[27] Leppkoski, H., et al. "Error Analysis of Step Length Estimation in Pedestrian Dead Reckoning." *Proc. ION GPS* 2002, Portland, OR, September 2002, pp. 1136-1142.

[28] Nike + iPod Sport Kit II information website. *http* : *//www.apple.com/ipod/nike/*. Apple Inc., last updated January 2009.